UNIVERSITY OF TURKU

Comparison of DNA damage biomarker dynamics after induced DNA damage

Study of DNA damage biomarker expression and dynamics in cancer cells

Drug Discovery and Development
Master's thesis

Author:
Sofia Forstén

Supervisors:
Julia Lindqvist, PhD
Johanna Ahlskog, PhD
Prof. Ullamari Pesonen, PhD

29.4.2022
Turku

Master's thesis

Subject: Drug Discovery and Development
Author(s): Sofia Forstén
Title: Comparison of dynamics of DNA damage biomarkers after induced DNA damage
Supervisor(s): PhD Julia Lindqvist, PhD Johanna Ahlskog, PhD Ullamari Pesonen
Number of pages: 76 pages
Date: 29.4.2022

To ensure genomic integrity and protect cells from a variety of DNA damaging agents, cells have developed a complex network called the DNA damage response (DDR). It monitors and ensures DNA integrity by coordinating DNA repair and activating cell cycle arrest to allow enough time for the repair. Loss-of function mutations of DNA repair factors can cause genetic disorders and increase susceptibility to cancer.

Cancer treatment with chemotherapeutic agents is based on the accumulation of DNA damage in cells, ultimately leading to cell death. Targeting the DNA damage response mechanisms by inhibiting specific proteins responsible for the DNA repair provides a more targeted treatment for specific cancer types. Currently there are four PARP inhibitors approved for the treatment of breast, ovarian and prostate cancer with *BRCA1/2* or *ATM* mutations. PARP inhibitors exploit the concept of synthetic lethality where cancer cells with the mutations rely on certain DNA repair pathways for survival. Despite the efficacy of PARP inhibitors, resistance to them has been described. This implies the need for new treatments, but also for better prognostic, diagnostic and pharmacodynamic biomarkers that could predict patient sensitivity to PARP inhibitors or to other targeted treatments.

For this study, five proteins that are involved in DNA double strand break (DSB) repair were chosen to be compared. The aim of this study was to compare the dynamics and expression of gamma-H2AX (phosphorylated yH2AX), phosphorylated replication protein A (pRPA), phosphorylated Kruppel-associated box (KRAB)3-associated protein 1 (pKAP1), tumor suppressor P53-binding protein 1 (53BP1) and DNA repair protein RAD51 homolog (RAD51), and to find the best biomarker among them and the best analysis method to be used in drug discovery purposes.

The dynamics and expression of the biomarkers were studied by inducing DNA DSBs with mitomycin C in DLD-1 parental and DLD-1 *BRCA2* knockout (KO) cells. The dynamics of each marker was also studied and compared after treating cells with PARP and ATR inhibitors. The spatiotemporal dynamics of these five markers was studied using fluorescence imaging and changes in protein levels were studied with Western blot.

These results indicate that there were differences between the markers in different conditions. To decide which of the markers was the best biomarker depended on the goal of the assay. To only determine the amount of DNA damage, yH2AX foci and 53BP1 foci number could be applied. If working with high concentrations of damaging agents then the increase in nuclear intensity in yH2AX, pRPA and pKAP1 signal could be used. RAD51 foci formation would be optimal for screening responsive cell lines to specific treatments or when analyzing the HR status of the cells.

To conclude, the results suggest that these proteins can be used as DNA damage biomarkers, but their wider use would still require further optimization. Depending on the goal, different marker and different analysis method will be optimal. Additionally, other cell lines should be added to the study to observe whether these results could be applied generally.

Key words: DNA damage response, DNA repair, *BRCA2,* biomarker

Table of contents

1 Introduction

1.1 DNA damage and repair

1.1.1 DNA damage response

Maintaining deoxyribonucleic acid (DNA) integrity is important to preserve genetic information and maintain cell and tissue homeostasis (Carrassa and Damia, 2017; Klinakis, Karagiannis and Rampias, 2020). Multiple different environmental agents can induce DNA damage in addition to spontaneous damage generated during DNA replication. To protect DNA integrity from damaging agents, cells have developed a complex network called the DNA damage response (DDR) (Carrassa and Damia, 2017). This network comprises of different intra- and intercellular events and enzyme activities. It monitors and ensures DNA integrity by coordinating the repair of DNA and activating cell cycle arrest to allow enough time for the repair. DNA damage can also lead to apoptosis or senescence if the repair is not optimal or not possible (O'Connor, 2015; Carrassa and Damia, 2017). Loss-of function mutations of DNA repair factors can cause genetic disorders and increase susceptibility to cancer (Klinakis, Karagiannis and Rampias, 2020).

Different types of DNA damage can be divided into endogenous and exogenous DNA damage (Chatterjee and Walker, 2017). Endogenous damage includes replication errors, DNA base mismatches, topoisomerase-DNA complexes, abasic sites and oxidative DNA damage caused by reactive oxygen species (ROS) that are created as a byproduct of multiple different biochemical reactions (Chatterjee and Walker, 2017). Exogenous DNA damage includes ionizing radiation (IR), ultraviolet (UV) radiation and different exogenous chemical agents. These chemical agents include for example alkylating agents, aromatic amines, and polycyclic aromatic hydrocarbon compounds. Exogenous DNA damage also includes different toxins and environmental sources of stress such as extreme heat or cold, hypoxia, and oxidative stress. (Chatterjee and Walker, 2017)

Recognition of the damage site initiates DDR signaling. Different DNA repair pathways are activated depending on the type of the damage (Jalal, Earley and Turchi, 2011) (Figure 1). Different DDR pathways can sometimes compensate for each other in the absence of the optimal one (Hoeijmakers, 2001; O'Connor, 2015).

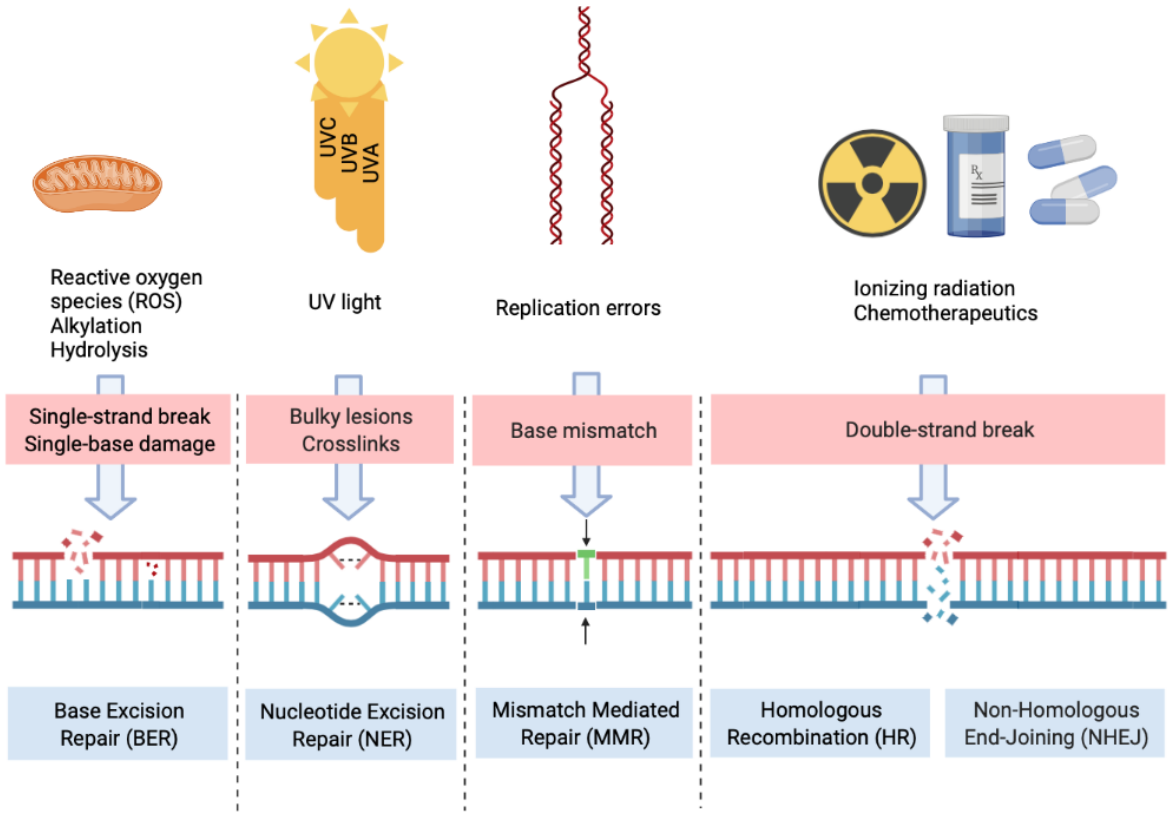

Figure 1. Schematic of different DNA damaging agents, DNA damage types and their repair pathways. Different types of DNA damage activate different DNA repair pathways. Single strand breaks caused by oxygen radicals, alkylating agents or spontaneous reactions are repaired with base excision repair. Bulky lesions and DNA crosslinks induced by UV light are repaired with nucleotide excision repair pathway. Mismatch errors generated during replication are repaired with mismatch repair. Double strand breaks caused by X-rays or antitumor agents are mainly repaired by homologous recombination or non-homologous end-joining. Adapted from (de Almeida et al., 2021). Created with BioRender.com.

1.1.2 Single strand break repair

The DNA mismatch repair (MMR) pathway mainly corrects replication errors that are caused by DNA polymerases during cell division (Hsieh and Yamane, 2008; Jalal, Earley and Turchi, 2011). These errors are base substitution mismatches and insertion-deletion mismatches (Jalal, Earley and Turchi, 2011). Defects in this repair pathway increase the mutation rate and susceptibility to cancer (Hoeijmakers, 2001). The main steps in this pathway are mismatch recognition, recruitment of the needed factors for the MMR, search for the wrongly synthesized strand, removal of the mismatch and resynthesis to correct the mismatch (Hoeijmakers, 2001).

Microsatellites, also called short tandem repeats are small 1 to 6 nucleotide repeats, distributed within the genome (Vaksman and Garner, 2015; Yang, Zheng and Jin, 2019). MMR functions also in maintaining the stability of these repeats (Hsieh and Yamane, 2008;

Vaksman and Garner, 2015; Yang, Zheng and Jin, 2019). Defects in MMR pathway due to mutations or epigenetic changes can lead to alterations in these repeats, which is a condition called microsatellite instability (MSI) (Hoeijmakers, 2001; Nojadeh, Sharif and Sakhinia, 2018; Yang, Zheng and Jin, 2019). MSI is associated with different cancer types, especially with colorectal cancers and with Lynch syndrome, which is an inherited predisposition to colon cancer (Hoeijmakers, 2001; Peña-Diaz et al., 2012; Vaksman and Garner, 2015; Yang, Zheng and Jin, 2019).

Base excision repair (BER) pathway repairs DNA base lesions (Jalal, Earley and Turchi, 2011). This type of damage is induced by oxidative agents, alkylation, deamination or depurination/depyrimidination (Hoeijmakers, 2001; Robertson et al., 2009). There are two general pathways of BER: short-patch and long-patch BER. Short-patch BER repairs single nucleotide damage and long-patch BER repairs damage of at least two nucleotides (Hoeijmakers, 2001; Robertson et al., 2009). BER pathway is initiated by DNA glycosylases recognizing the damaged bases and removing them. This is followed by strand incision, gap-filling and ligation done by different downstream enzymes (Robertson et al., 2009). Oxidative damage and its repair through BER are linked to different disorders as well. As DNA damage caused by oxidative stress accumulates over time, especially diseases of aging such as cancer and neurodegenerative disorders, can be linked to BER at least to some extent (Wallace, 2014).

Nucleotide excision repair (NER) pathway recognizes and repairs larger, helix-distorting lesions. These bulky DNA lesions are caused by chemical modifications of DNA that can be caused by environmental mutagens such as UV-light, tobacco smoke or chemotherapeutic agents. There are two sub-pathways of the NER: transcription coupled NER (TC-NER) and global genomic NER (GG-NER) (Hoeijmakers, 2001; Jalal, Earley and Turchi, 2011). These pathways differ from each other in the initial recognition step of the damage and by their substrate specificity: global genome NER guards the whole genome for these lesions, whereas transcription coupled NER focuses on damages that interfere with elongating RNA polymerases (Hoeijmakers, 2001).

Inborn defects in NER are associated with a few disorders that are characterized by exquisite sun sensitivity. The main disorder linked to NER is xeroderma pigmentosum (XP). XP is a photosensitivity syndrome characterized by a very high incidence of light-induced skin cancer. XP is caused by mutations in one of seven genes (e.g. XPA, XPG) which carry out the

excision repair (Hoeijmakers, 2001; Sancar et al., 2004). Modest elevation in incidence of other cancer types is associated with XP as well (Hoeijmakers, 2001).

1.1.3 Double strand break repair

Double-strand breaks (DSBs) are the most threatening type of damage to genomic integrity and to cells overall. SSBs can develop into DSB in the cell division if left unrepaired. In addition, DSBs can be caused by endogenous or exogenous agents. Endogenous damaging agents include ROS generated during cellular metabolism, collapsed replication forks or damage by nucleases. DSBs can also be programmed as in immune system maturation or in meiosis (Prakash et al., 2015; Ranjha, Howard and Cejka, 2018). In T and B lymphocyte development, the random rearrangement of the variable (V), diversity (D), and joining (J) segments of immunoglobulin genes results from DNA DSBs. And their repair is needed to produce the different antigen receptors (Ranjha, Howard and Cejka, 2018). Exogenous damaging agents include ionizing radiation and different DNA damaging chemicals, both direct and indirect damage-causing agents such as chemotherapeutic agents (Shrivastav, de Haro and Nickoloff, 2008). DSBs can also be a result of chromosome breakage or telomere deprotection (Scully et al., 2019). If DSBs are left unrepaired or repaired incorrectly, they can result in cell death or different genetic alterations. DSBs can result in large- or small-scale deletions, loss of heterozygosity, translocations and even chromosome loss. These disrupted gene structures and functions can also lead to different hereditary diseases or tumorigenesis (Shrivastav, de Haro and Nickoloff, 2008; Ceccaldi, Rondinelli and D'Andrea, 2016; Ranjha, Howard and Cejka, 2018; Scully et al., 2019).

Repair of DSBs is mediated by different pathways that can compensate for each other if needed to minimize the genomic damage (Scully et al., 2019). Two main pathways that correct DSBs are homologous recombination (HR) pathway and non-homologous end-joining (NHEJ) pathway (Jalal, Earley and Turchi, 2011). NHEJ is a rapid pathway that can join the two DNA ends with minimal reference structure. HR, on the contrary requires, high sequence homology and a template strand to repair the DSB (Scully et al., 2019). HR is considered almost error-free repair and it gives rise to minimal mutation potential in normal conditions, whereas NHEJ has more potential to give rise to mutations and malignancies (Her and Bunting, 2018). There are also two more error prone pathways that repair DSBs: single-strand annealing (SSA) pathway and alternative end joining (alt-EJ) pathway (Ceccaldi, Rondinelli and D'Andrea, 2016; Scully et al., 2019).

SSA uses homologous repeats in the DSB site to join the two DNA ends. It involves DNA end resection to reveal the repetitive sequences and therefore it causes nucleotide deletions and is considered a relatively mutagenic repair pathway. (Ceccaldi, Rondinelli and D'Andrea, 2016; Ranjha, Howard and Cejka, 2018) Alt-EJ, also called microhomology-mediated end joining (MMEJ), repairs DNA DSBs by ligating microhomologies which are 2 to 20 nucleotide long (Ceccaldi, Rondinelli and D'Andrea, 2016; Ranjha, Howard and Cejka, 2018; Seol, Shim and Lee, 2018).

NHEJ and HR are less mutagenic than SSA and Alt-EJ. Which of the repair pathways is activated, depends on the cell cycle phase and on the end resection of the damaged site in the DSB. NHEJ is thought to operate throughout the cell cycle but is dominated in G0/G1 phase (Ceccaldi, Rondinelli and D'Andrea, 2016), whereas HR is restricted to cell cycle phases, where template for the homology repair is available. HR is thus restricted to S and G2 phases (Shrivastav, de Haro and Nickoloff, 2008; Ceccaldi, Rondinelli and D'Andrea, 2016; Scully et al., 2019).

NHEJ initiates when a Ku70-80 (XRCC6-XRCC5) heterodimer detects the DSB and binds to the free DNA ends (Jachimowicz, Goergens and Reinhardt, 2019; Scully et al., 2019). It recruits then other NHEJ factors including the catalytic subunit of DNA-dependent protein kinase (DNA-PKcs), DNA ligase IV and different scaffolding factors (Scully et al., 2019). In NHEJ, blunt DSB ends are ligated together without sequence homology (Ceccaldi, Rondinelli and D'Andrea, 2016). If the ends cannot be straightly joined, NHEJ involves alignment of few nucleotides. This can lead to small deletions or insertions. (Shrivastav, de Haro and Nickoloff, 2008) NHEJ has a great role in preserving genome integrity as with it, chromosomal translocations and other large chromosomal aberrations can be avoided (Ceccaldi, Rondinelli and D'Andrea, 2016).

Homologous recombination requires high sequence homology from the template used in the repair. Templates that can be used are sister chromatids or homologous chromosomes (Shrivastav, de Haro and Nickoloff, 2008). HR pathway is initiated with processing of the broken ends of the DSB by the MRE11/RAD50/NBS1 (MRN) complex and C-terminal binding protein 1 (CtBP1) interacting protein (CtIP) endonuclease (Sartori et al., 2007; Shrivastav, de Haro and Nickoloff, 2008; Ceccaldi, Rondinelli and D'Andrea, 2016; Lu and Davis, 2021). This DNA resection results in long 3' ssDNA overhangs where ssDNA-binding protein replication protein A (RPA) rapidly binds (Shrivastav, de Haro and Nickoloff, 2008;

Zhao et al., 2015; Ceccaldi, Rondinelli and D'Andrea, 2016; Lu and Davis, 2021). RPA is then quickly replaced by DNA repair protein RAD51 homolog (RAD51) (Shrivastav, de Haro and Nickoloff, 2008; Ceccaldi, Rondinelli and D'Andrea, 2016). RAD51 forms a helical nucleoprotein filament with the ssDNA and this filament then searches for a homologous DNA sequence. The strand exchange directed by RAD51 is the defining step of HR and specific for HR. Thus, after that the repair is committed to HR (Prakash et al., 2015). Once a sufficient pairing and homology is identified, DNA synthesis can be done by DNA polymerases and ligases (Ranjha, Howard and Cejka, 2018; Wright, Shah and Heyer, 2018; Scully et al., 2019; Lu and Davis, 2021). Details and differences of NHEJ and HR are presented in Figure 2.

1.1.4 BRCA1 and BRCA2 function in HR and cancer predisposition

Even tough HR is an important pathway to promote genomic stability it is also connected to human cancer risk especially through involvement of hereditary cancer predisposition genes, breast cancer gene 1 and 2 (BRCA1 and BRCA2) (Cruz et al., 2018; Scully et al., 2019). They encode for BRCA1 and BRCA2 proteins that have important roles in HR. Mutations in those genes lead to defects in HR and a rise in genomic instability and therefore predispose to certain cancers (Prakash et al., 2015; Cruz et al., 2018).

BRCA1 and BRCA2 proteins assure the efficient and precise repair of DSBs during HR (Gudmundsdottir and Ashworth, 2006). BRCA1 acts first in 5´to 3´end resection to create the 3' overhangs which are later coated by RPA. BRCA1 also promotes this end resection by antagonizing the resection inhibitor Tumor suppressor P53-binding protein 1 (53BP1) and regulating the MRE11–RAD50–NBS1–CtIP resection nuclease complex. BRCA1 also promotes the RAD51-mediated homologous DNA pairing (Prakash et al., 2015). Later it helps BRCA2 to load RAD51 onto the ssDNA through Partner and Localizer of BRCA2 (PALB2) which acts as a bridging protein (Prakash et al., 2015; Zhao et al., 2017). BRCA2 is directly involved in RAD51-mediated repair, and it promotes the loading of RAD51 which is essential for the HR and guides the repair to HR instead of more mutagenic pathways (Stark et al., 2004; Gudmundsdottir and Ashworth, 2006; Prakash et al., 2015).

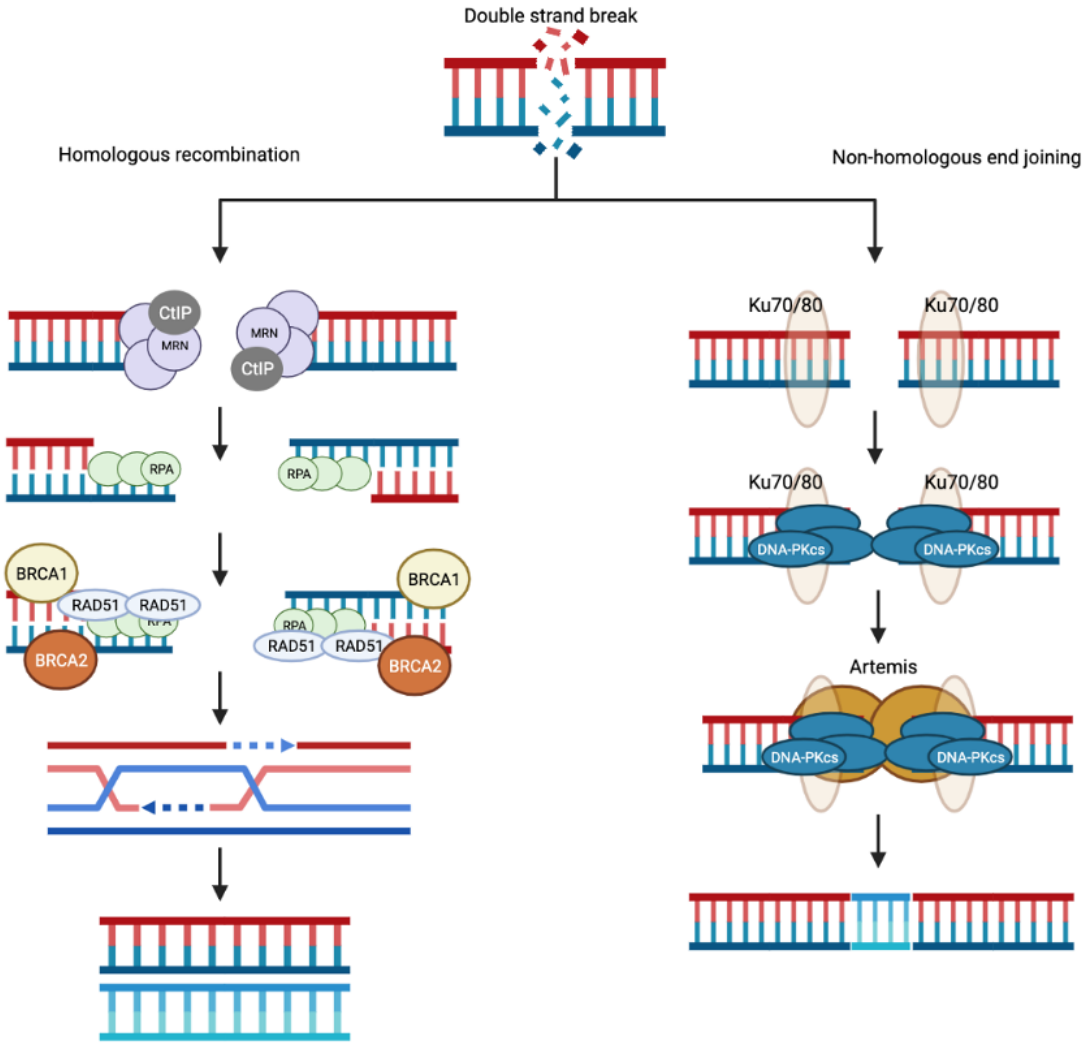

Figure 2. Details of non-homologous end-joining and homologous recombination. NHEJ is initiated when Ku70-80 (XRCC6-XRCC5) detects the DSB and binds to the broken ends. It then promotes other factors including DNA-PKs, ligases, and other scaffolding factors to ligate the ends. HR is initiated with the MRN complex processing the free ends of the DSB with the help of CtIP. RPA is rapidly bound to ssDNA hangs but is quickly replaced by RAD51. The formed nucleoprotein filament then searches for homologous sequence and when sufficient pairing is identified the DSB is repaired by DNA polymerases and ligases. Adapted from (Nesic et al., 2018). Created with BioRender.com.

1.2 DNA damage markers

There are several proteins identified that could be used as biomarkers for DNA damage. For this project gamma-H2AX (yH2AX; phosphorylated histone variant H2AX), phosphorylated Replication protein A (pRPA), phosphorylated Kruppel-associated box (KRAB)3-associated protein 1 (pKAP1), Tumor suppressor P53-binding protein 1 (53BP1) and DNA repair protein

RAD51 homolog (RAD51) were chosen and will be collectively called DNA damage biomarkers in this study.

One of the earliest responses to DSB is phosphorylation of histone variant H2AX. H2AX is one of three types of histone H2A molecules that are present in eukaryotic cells and package DNA into dense chromatin structure (Redon et al., 2010). H2AX is phosphorylated on Serine 139 in its carboxyl terminal tail, and this phosphorylated H2AX is called gamma-H2AX (yH2AX) (Stiff et al., 2004). yH2AX is phosphorylated byseveral kinases: ataxia telangiectasia mutated (ATM) kinase, ATM and Rad3-related (ATR) kinase and DNA-dependent protein kinase (DNA-PK) (Burma et al., 2001; Podhorecka, Skladanowski and Bozko, 2010). ATM is considered to be the main mediator of yH2AX phosphorylation. Upon DNA damage, ATM is autophosphorylated, which leads to activation of the kinase. In the case of DSB, many different DDR proteins relocate and form nuclear supramolecular structures, called foci, at sites of DNA damage. For example, MRN complex, MDC1, 53BP1 and BRCA1 form foci at DSBs. These proteins interact with yH2AX and other proteins leading to more DDR factors accumulating to the DSB site. The MRN complex recruits ATM to the damaged site and helps ATM to target its activity to correct substrates (Lowndes and Toh, 2005; Podhorecka, Skladanowski and Bozko, 2010). The exact function of yH2AX in DSB repair is not completely elaborated, however, the attraction of other DDR proteins to the damage site by providing a platform for the accumulation of proteins to the site may be the most relevant contribution of yH2AX to DNA repair (Kinner et al., 2008; Ding et al., 2016).

Replication protein A (RPA) is a protein that binds to ssDNA and is involved in DNA replication, DNA repair and recombination (Wang et al., 2001; Block, Yu and Lees-Miller, 2004). It is a heterotrimer of 70, 32 and 14 kDa subunits. In response to DNA damage, the 32 kDa subunit of RPA (RPA32) is phosphorylated (pRPA) by ATM and DNA-PK (Block, Yu and Lees-Miller, 2004). It has been shown that RPA32 hyperphosphorylation mediates the recruitment of DDR proteins at the damage sites and is involved in the regulation of HR and thereby promotes genome stability (Vassin, Wold and Borowiec, 2004; Shi et al., 2010; Byrne and Oakley, 2019). pRPA also has other functions in the replication fork. It prevents secondary structures by binding to the single stranded lagging strand and promotes the priming activity of the lagging strand (Bhat and Cortez, 2018).

Tumor suppressor P53-binding protein 1 (53BP1) is a chromatin binding protein and a member of the Tudor-containing proteins that act as histone methylation readers

(Noordermeer et al., 2018; Mirza-Aghazadeh-Attari et al., 2019). It is a transducer in DDR, and it senses the damage and interacts with other important mediators such as ATM, BRCA1 and tumor protein p53 (Noordermeer et al., 2018; Mirza-Aghazadeh-Attari et al., 2019). It also has a critical role in choosing DSB repair pathway, as it promotes the NHEJ pathway over HR pathway in G1 by counteracting the function of BRCA1 (Panier and Boulton, 2014; Ding et al., 2016; Mirza-Aghazadeh-Attari et al., 2019). 53BP1 is first recruited to the DSB site by Mediator of DNA Damage Checkpoint 1 (MDC1) and it is then retained in the damage area by interaction with histone H4 which is dimethylated on lysine 20 (H4K20me2) (Daley and Sung, 2014; Mirza-Aghazadeh-Attari et al., 2019). It has also been shown that Ring finger proteins 8 and 168 (RNF8 and RNF168) that are ubiquitin E3 ligases are necessary for the recruitment of 53BP1 (Daley and Sung, 2014). 53BP1 amplifies ATM activity to promote checkpoint signalling in response to low levels of DNA damage.

Kruppel-associated box (KRAB)3-associated protein 1 (KAP1) is a universal transcriptional co-repressor for Krüppel-associated box zinc finger proteins (KRAB-ZFPs) (Magni et al., 2015). KAP1 is required for the induction of heterochromatin relaxation during DNA replication and DNA repair (Magni et al., 2015; Jang et al., 2018). KAP1 also regulates multiple physiological aspects including cell differentiation, DNA damage response, virus replication, immune response, and tumorigenesis (Cheng, 2014). In response to DNA damage KAP1 is phosphorylated at serine 473/824 sites (pKAP1) by ATM and ATR (Hu et al., 2012; White et al., 2012). This phosphorylation leads to local relaxation of heterochromatin at the DSB sites, giving access to the repair machinery (Noon et al., 2010; Ding et al., 2016).

DNA repair protein RAD51 homolog (RAD51) is, like RPA, a DNA-binding protein that helps to maintain genome stability during DNA replication (Bhat and Cortez, 2018). As discussed previously in the HR pathway section (Section 1.1.3), RAD51 rapidly replaces RPA on ssDNA ends and forms nucleoprotein filaments on the ssDNA with different DNA binding mechanisms. Which together with D-loop formation are fundamental for error-free HR (Laurini et al., 2020). The primary mediator of this function is BRCA2. BRCA2 helps to displace RPA and load RAD51 to the ssDNA overhangs. RAD51 paralogs cooperate with BRCA2 and promote the formation and stabilization of the filaments (Bhat and Cortez, 2018; Laurini et al., 2020).

1.3 Regulators of DNA damage response

The key regulators of DDR are three kinases from phosphatidylinositol 3-kinase (PI3K) -like protein kinases (PIKKs); ATM, ATR, and DNA-PK (Shiloh, 2003; Stiff et al., 2004). These kinases are recruited to the damage site by different protein complexes; ATM is recruited by MRE11/RAD50/NBS1 complex, ATR is recruited by RPA and KU70-KU80/86 recruits DNA-PKcs (Menolfi and Zha, 2020). After recruitment and their activation, these kinases phosphorylate their substrates and promote efficient and accurate DNA repair (Menolfi and Zha, 2020).

ATM is the first kinase to react to DSB by phosphorylating its substrates. Phosphorylation of these substrates can either activate or repress the activity depending on the substrate (Shiloh, 2003). The main substrates of ATM are checkpoint kinase 1 and 2 (CHK1/2), BRCA1, 53BP1 and MDC1 (Stiff et al., 2004). The binding of ATM to MRN complex generates the signal for yH2AX leading to recruitment of other DDR factors (Brown et al., 2017). Mutation in ATM causes a rare hereditary disorder ataxia telangiectasia (Stiff et al., 2004).

ATR is responsible for phosphorylation of many of the same substrates as ATM. In DSB repair, ATM reacts first, but ATR is later recruited to the damage site by RPA where it then maintains the phosphorylation state of specific substrates. (Shechter, Costanzo and Gautier, 2004) This enables fine-tuning of DSB repair. ATR is the main kinase in ssDNA breaks, such as stalled replication forks (Shiloh, 2003). The main substrate of ATR is CHK1 which inhibits cyclin-dependent kinase (CDK) activity by phosphorylating the CDK1's key regulators, resulting in CDK1 inactivation and blockade of G2/M transition (Patil, Pabla and Dong, 2013; Brown et al., 2017). DNA-PKs are mainly acting in NHEJ not in HR (Shiloh, 2003).

1.4 DNA damage response in cancer

1.4.1 Cancer susceptibility

Pre-cancerous cells can have deregulated cell cycle control and increased replication stress, leading to DNA damage and genomic instability, which is one of the hallmarks of cancer (Hanahan and Weinberg, 2011; O'Connor, 2015; Klinakis, Karagiannis and Rampias, 2020). Deficiency several DNA repair genes is connected to human cancer risk. Well-known examples are the tumor-suppressor genes BRCA1 and BRCA2 (Scully et al., 2019). These genes encode essential proteins for HR, as discussed earlier (section 1.1.4), and loss-of function mutations lead to impairment of the repair pathway. This condition can be called as

homologous recombination deficiency (HRD). This can lead to genomic instability, and therefore, to increased risk of especially breast and ovarian cancers (Prakash et al., 2015; Cruz et al., 2018; Scully et al., 2019).

In addition to BRCA1/2 also mutations in RAD51-, ATM- and ATR -genes are linked to increased cancer risk. Mutations directly in RAD51 or in its regulators have effects on genome stability leading to cancer or Fanconi anemia-like syndrome (Grundy, Buckanovich and Bernstein, 2020). Especially mutations in RAD51 are linked to breast and ovarian cancers (Grundy, Buckanovich and Bernstein, 2020). Mutations in ATM and ATR can lead to, in addition to Ataxia-Telangiectasia and Seckel syndrome, to genome instability and drive carcinogenesis (Waskiewicz et al., 2021).

1.4.2 Cancer treatments exploiting DNA damage response

Traditional anticancer therapies either with chemotherapeutic agents or radiation therapy are based on the accumulation of DNA damage in rapidly proliferating cells, which ultimately leads to cell death. This approach, however, lacks selectivity and the systemic response leads to the wide range of unwanted adverse events (Redon et al., 2010; O'Connor, 2015). Targeting the DDR mechanisms by inhibiting specific proteins responsible for DNA repair would provide a more targeted treatment for specific cancer types (O'Connor, 2015).

The concept of synthetic lethality, which was first described already in 1920s (Bridges, 1922; Dobzhansky, 1946), refers to situation where "co-occurrence of two genetic events results in organism or cellular death" (Nijman, 2011). In context of cancer, the inactivation of DNA repair components due to mutations, like BRCA1/2 mutations, lead to deficiency in DNA repair. Cancer cells then become dependent on the remaining pathways and thus synthetic lethality can be exploited by inhibiting the new dependency. This allows specific targeting of cancer cells over normal cells (Curtin, 2012; Klinakis, Karagiannis and Rampias, 2020).

Exploitation of DDR defects by synthetic lethality is thus a promising approach for cancer therapy as has already been proved with poly(ADP-ribose) polymerase (PARP) inhibitors in BRCA1/2 mutated cancers that are defective in HR (Curtin, 2012) (Figure 3). Cancer cells with BRCA1/2 mutation rely on NHEJ and alt-EJ, which require PARP1 in the initiation of the repair. PARP1 is recruited to the damage site where it adds chains of ADP-ribose residues (PAR chains) onto the damage site. These chains facilitate other repair proteins to be recruited to the site of damage and the repair cascade to be activated. Hence, PARP1 functions as a

sensor for DNA damage and it recognizes SSBs, repairs DSBs and stabilizes replication forks. At SSBs, PARP1 aids the repair and inhibits the SSBs from developing into DSB (Curtin, 2012; Pommier, O'Connor and de Bono, 2016).

PARP inhibitors (PARPi) inhibit the recruitment of repair proteins and lead to accumulation of PAR molecules at the damage site and ultimately increase the damage burden of the cells that eventually leads to cell death (Cruz et al., 2018; Klinakis, Karagiannis and Rampias, 2020; Janysek et al., 2021). Some of the PARP inhibitors are also called PARP trappers. They trap the PARP enzyme on DNA and therefore prevent the repair of the damage (Murai et al., 2012; Zheng et al., 2020). Figure 3. presents a schematic of PARP inhibitors' mechanisms of action and synthetic lethality in HR deficient tumors. The defects in HR also increase the sensitivity of BRCA-mutated tumors to different traditional DNA damaging agents, like anthracyclines or platinum salts (Cruz et al., 2018; O'Connor, 2015; Patel, Algouneh and Hakem, 2021). Patients with other mutations leading to HRD can also benefit from these treatments. A term "BRCAness" can be used to define these cancers that lack BRCA mutations but bear a similar DNA-repair defect phenotype (Gou, Dong and Lin, 2020).

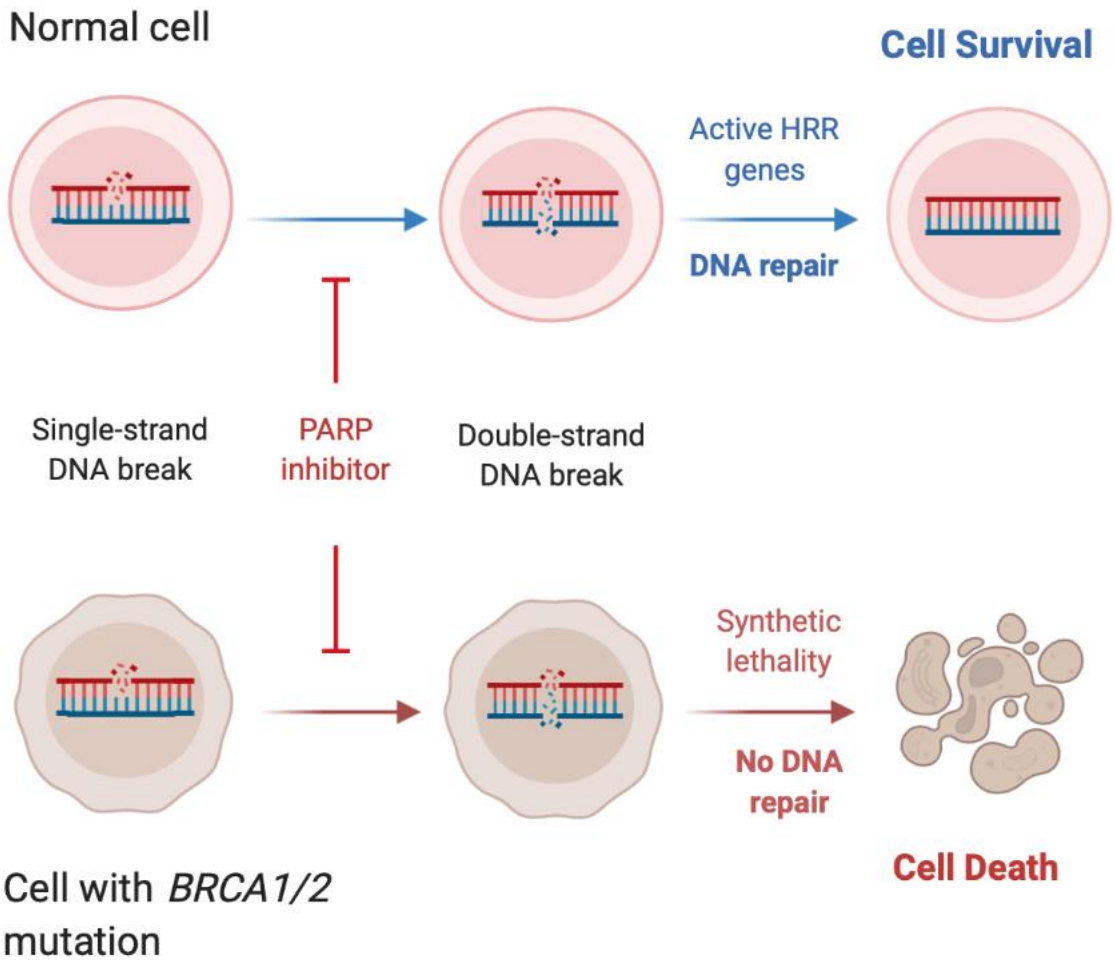

Figure 3. PARP inhibitors' mechanisms of action. PARP inhibitors exploit the concept of synthetic lethality in cancer. In cells with intact HR the inhibition of PARP does not lead to cell death as there are other repair pathways that compensate for the lost one. Cells that have deficiency in HR, however, rely on NHEJ and alt-EJ in DSB repair. These pathways require PARP1, and its inhibition leads to cell death. Adapted from "PARP Inhibitors: Treatment For BRCA Mutant Breast Cancer", by BioRender.com (2022). Retrieved from https://app.biorender.com/biorender-templates.

In addition to PARP inhibitors, other drugs targeting DNA repair proteins are in development. For example, inhibitors have been developed against ATM, ATR, DNA-PK, WEE1 G2 Checkpoint Kinase (WEE1) and CHK1 and 2. There are also several different strategies for combination therapies, for example combining PARP inhibitors with chemotherapeutic agents or with radiation, in clinical trials (Carrassa and Damia, 2017).

ATR has an important role in controlling the G2/M checkpoint. This prevents the cells' entry into mitosis if the cell is damaged or the DNA damage cannot be repaired (Barnieh, Loadman and Falconer, 2021). Following this its inhibition has quite great potential to be used as cancer therapeutic. In addition, cancer cells often have loss of G1 checkpoint control, making them

more reliant on the G2/M checkpoint (Bradbury et al., 2020). Targeting ATR has potential in cancer treatment either as monotherapy or in combination with chemotherapy, radiotherapy, and immunotherapy. Inhibiting ATR has been shown to increase the sensitivity of tumor cells to genotoxic agents, increase cell death or increase cellular senescence (Barnieh, Loadman and Falconer, 2021). ATR's downstream effector molecule CHK1 also suppresses replication stress by inhibiting excess initiation of DNA replication. CHK1 inhibitors are also in preclinical and early clinical trials (Qiu, Oleinick and Zhang, 2018).

As discussed, ATM has an important role in activating DNA repair. By inhibiting ATM kinase activity, and therefore inhibiting DNA repair, tumor cells have been shown to be more sensitive to radiation and chemotherapy (Lavin and Yeo, 2020). At this point there are few ATM inhibitors under development in preclinical and early clinical phases, both as monotherapy and as a combination therapy (Carrassa and Damia, 2017).

WEE1 is a tyrosine kinase that inhibits activation of Cyclin-dependent kinase 1 (CDK1) and Cyclin-dependent kinase 2 (CDK2) and thus regulates cell cycle by regulating G2/M and S phases which are important in DDR. Inhibition of WEE1 increases replication stress and genomic instability which can enhance the effects of other drugs targeting DDR like PARP inhibitors (Ha et al., 2020).

1.5 Biomarkers of DNA damage response and their potential use in diagnostics and in drug development

Deficiencies in DNA repair may result in DNA aberrations that can help in distinguishing HR deficient tumors from HR proficient. These genomic scars are not, however, always that clear and the aberrations may persist even after the HR function is restored (Cruz et al., 2018). Thus there is an evident need for specific biomarkers that can be used to identify defects in DDR. These predictive biomarkers could be used to select the right patients for the right therapy or to detect resistance to certain therapies (Curtin, 2012; Cruz et al., 2018). There is also need for pharmacodynamic biomarkers that could be used in drug development to efficiently study the effect and selectivity of a DDR targeting drug (Curtin, 2012; Ceccaldi, Rondinelli and D'Andrea, 2016; Cleary et al., 2020). These markers could either indicate cells with DNA damage or cells that have active damage repair system but may not always be predictive of overall drug response (Wilsker et al., 2019).

There are few examples of studies of predictive biomarkers. There is, for example, some evidence that induction of RAD51 foci in biopsy samples after irradiation predicts treatment

response to chemotherapy in breast and ovarian cancer tumors (Cruz et al., 2018). It has been observed that RAD51 foci detection correlates with functional or restored HR functions in tumor cells and predicts resistance to PARP inhibitors (Cruz et al., 2018). This suggests that RAD51 foci levels could be used as an alternative approach to BRCA1/2 testing to identify genomic defect in HR (Curtin, 2012).

Increase of yH2AX is a general marker of DNA damage. It can be used to observe DNA damage levels before and after patient treatment but also in vitro to study DNA damage (Redon et al., 2010; Curtin, 2012). Furthermore, a panel of multiple biomarkers together could be used to assess the cellular pharmacodynamic response to different drugs. For example, a panel of γH2AX, 53BP1 and RAD51 has been studied (Wilsker et al., 2019; Willers et al., 2015).

Even though these markers represent DNA damage and may help in recognizing correct patients to correct treatments, it should be noted that they do not directly measure the DNA damage. They can be used to detect the DNA damage and their repair but are not exact.

1.6 Summary and aims of the research

Maintaining genomic integrity is the purpose of the DNA damage response. The greatest threat to genome is DNA double strand breaks and the main linked repair pathways are HR and NHEJ. HR is the most accurate repair mechanism as it uses a homologous template in the repair. Different sensor- and effector proteins work together in DDR and these proteins can also be used as biomarkers of DNA repair. Defects in DNA repair factors can cause genetic disorders and increase susceptibility to cancer.

Traditional anticancer treatments are based on the accumulation of DNA damage in rapidly proliferating cells. Due to large number of unwanted adverse events, more targeted therapeutics are needed. Synthetic lethality is the main mechanisms that is now studied and applied to cancer therapy. PARP inhibitors are a great example of this. Four PARP inhibitors are currently approved for clinical use: olaparib, rucaparib, niraparib, and talazoparib. These are approved for the treatment of breast, ovarian and prostate cancer with *BRCA1/2* or *ATM* mutations. Despite the efficacy of PARP inhibitors, acquired resistance to them has been described occurring through different mechanisms. PARP resistance can rise for example by restoration of BRCA1-BRCA2 axis, up-regulation of RAD51, down-regulation of NHEJ or upregulation of drug efflux pumps (Janysek et al., 2021). Some patients with *BRCA1/2*

mutations do not respond to PARP therapy at all. This implicates the need for new treatments, but also for better prognostic, diagnostic and pharmacodynamic biomarkers that could predict patient sensitivity to PARP inhibitors or to other treatments. There is also need for these biomarkers in the drug discovery processes.

In this project, the aim was to find the best biomarker or biomarkers, and the best analysis method that could be used in drug discovery and development purposes using imaging approach. A good marker could be used as a pharmacodynamic biomarker representing the DDR activation and extent of DNA damage in cancer cells.

An isogenic cell pair was used in this study; DLD-1 parental cell line which is capable to repair DSBs by HR and DLD- 1 *BRCA2 -/-* cell line which is HRD. Cells were treated with alkylating agent, mitomycin C, with concentrations of 1 nM to 1 μM for 16 h, to induce double strand breaks, and the dynamics and expression of yH2AX, pRPA, 53BP1, pKAP1 and RAD51 were studied at different timepoints with immunofluorescence imaging. Cells were also treated with three PARP inhibitors and two ATR inhibitors to observe how these compounds affect the markers' dynamics. In addition, changes in dynamics at protein levels were confirmed with Western blot. Based on literature, all these markers are highly expressed during DNA damage repair and could be used as biomarkers. However, they had not been compared to each other in this manner and their dynamics and expression had not been completely elaborated under current conditions.

Results from this study could be applied to drug discovery processes as these markers could be used as pharmacodynamic biomarkers representing the DDR response and the HR status of cancer cells. Best biomarker and suitable image analysis method could be applied to drug screening or when testing cells' responses to DDR inhibitors. These results could be useful when analysing the effects of target gene knockdown or inhibition. In the future, these markers could possibly be used to predict drug response or susceptibility to resistance from patient samples.

2 Results

2.1 Optimization of experiment conditions

Different optimizations of experiment conditions were conducted before the final experiments. Summary of all optimalizations and their outcomes are presented in Table 1.

Table 1. Optimizations of experiment conditions.

Experiment	**Optimization/tested conditions**	**Outcome**
Optimization of fixing protocol	Comparing fixation with 3.7 % Paraformaldehyde (PFA) or methanol	Fixing with methanol or PFA did not show clear differences and fixation protocol with 3.7% PFA was chosen.
Optimization of primary antibodies	Testing three different concentrations of each antibody	Selected final concentrations of each primary antibody
Optimization of secondary antibodies	Due high background signal Alexa Fluor™ 488 and Alexa Fluor™ 568 were compared	Alexa Fluor™ 488 was chosen
Applying pre-extraction protocol before fixing to washout the cytoplasmic fraction of the cells. Pre-extraction was performed to study whether the nuclear foci of chromatin-bound proteins would be better visualized in immunofluorescence imaging.	Fixing with PFA or methanol with and without pre-extraction step	Pre-extraction led to loss of too many cells, continuation without pre-extraction step was chosen
Optimization of imaging conditions	Imaging with 20x and 63x objectives	All foci were visible only with using 63x objective
Optimization of western blotting	Loading different protein amounts of samples and testing different antibodies and concentrations	20 ug of protein was decided to be good amount of sample to be loaded to gel. Final antibodies and dilutions were determined. Decided to exclude 53BP1 from western blotting analysis due the high molecular weight and difficulties in blotting and visualization.
Optimization of mitomycin C (MMC) conditions, concentrations and timepoints for IF imaging	Testing two conditions: continuous MMC treatment and washout experiment, where MMC is washed away from cells after 16 h treatment.	Continuous MMC treatment up to 72 h caused cell death. Decided that this does not answer questions of interest. With high concentrations of MMC (µM range), washout

Experiment	Optimization/tested conditions	Outcome
		wasn't adequate to rescue cells after 48 h. With concentrations around IC50 value (nM range) of MMC, cells survived in all timepoints.

2.2 Proliferation assay to determine IC50 values

A six-day proliferation assay with MMC, PARP inhibitors (olaparib, veliparib, rucaparib) and ATR inhibitors (elimusertib, ceralasertib) (ATRi) was performed to obtain IC50 (half maximal inhibitory concentration) values for each compound. IC50 values were determined to find appropriate working concentrations for each experiment. This proliferation assay was also performed to ensure the functional consequence of the BRCA2 knockout as a response to PARP inhibitors. Both cell lines responded to ATR inhibitors and MMC, but as expected parental cells showed modest response to PARP inhibitors whereas the BRCA2 knockout cell line (KO cells) had a clear response (Figure 4). IC50 values obtained from proliferation assay are listed in Table 2.

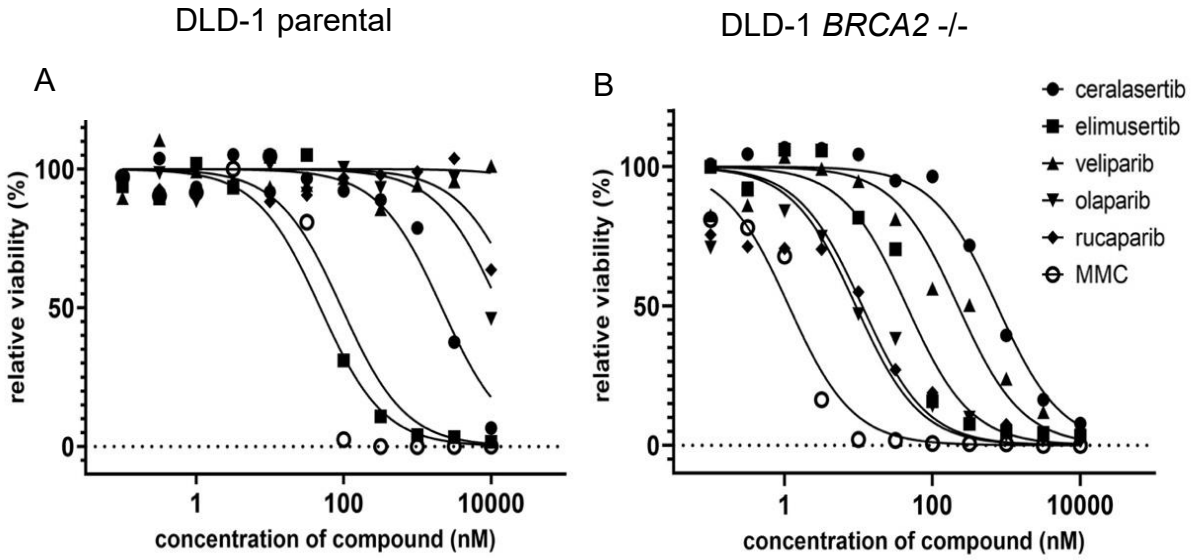

Figure 4. Six-day proliferation assay was performed to obtain IC50 values for MMC, ATR inhibitors (ceralasertib and elimusertib), and PARP inhibitors (veliparib, olaparib and rucaparib). A serial dilution curve starting from 10 µM with 3.162 dilution factor was used with all compounds. Dose-response curves were normalized to 0.1 % DMSO (100% viability) and 10 µM MMC (0% viability). (A) Dose-response of DLD-1 parental cells shows that the cells responded to ATR inhibitors and MMC, but not to PARP inhibitors. (B) Dose-response of DLD-1 *BRCA2* KO cells shows response to all compounds.

Table 2. IC50 values (nM) of compounds used in this project.

Compound	**IC50 in DLD-1 parental cells**	**IC50 in DLD-1 *BRCA2 -/-***
Mitomycin C	48 nM	1.5 nM
Ceralasertib	2100 nM	750 nM
Elimusertib	93 nM	45 nM
Olaparib	> 10,000 nM	12 nM
Rucaparib	> 10,000 nM	10 nM
Veliparib	> 10,000 nM	225 nM

2.3 Immunofluorescence imaging to study expression and dynamics of DNA damage makers

To study the expression and dynamics of the DNA damage markers, cells were treated with MMC to chemically induce DSB. Cells were treated with DMSO, 1 nM MMC, 10 nM MMC or 1000 nM MMC for 16 h followed by a medium change. Cells were fixed at different timepoints after washout. Representative immunofluorescence images of all biomarkers at 24 h timepoint post washout are shown in Figure 5 and 6. Image parameters were determined separately for each antibody and fluorescence intensities cannot be compared between different antibodies.

Dose-dependent increase in nuclear fluorescence signal intensity was observed with yH2AX. With pKAP1, induction was only acquired with 1000 nM MMC; with low concentrations, no signal was obtained. Marked changes in nuclear intensities with pRPA, 53BP1 or RAD51 could not be seen (Figures 5 and 6).

Nuclear foci formation was visible with yH2AX, 53BP1 and RAD51. In these experiments, pRPA and pKAP1 did not form nuclear foci. Dose-dependent increase in foci formation was seen after MMC treatment with yH2AX, 53BP1 and RAD51. Also, already at 24 h timepoint a clear increase in the nuclear size can be visually observed in both cell lines after 1000 nM MMC treatment (Appendix 1). Images were analysed in Columbus and visualised using GraphPad Prism (quantitative measurements of fluorescence signal intensity from the nuclear area and the formation of nuclear foci) (Figures 7 to 11).

yH2AX showed a clear increase in signal intensity with higher MMC concentration. With 1 nM and 10 nM MMC the signal decreased at later timepoints, whereas the signal increased

throughout all timepoints after 1000 nM MMC treatment (Figure 7A). With 1000 nM MMC, signal intensity increased more in KO cells than in parental cells in the two last timepoints (Figure 7B). Equally, in foci formation analysis, more foci per cell were observed with higher concentration of MMC. Increase was clear in parental cells, whereas in KO cells, 10 nM MMC was already enough to yield the maximal number of observed foci (Figure 7C, D). Foci was also decreasing at later timepoints with the two lower doses of MMC in both cell lines. After 1000 nM MMC treatment the foci number decreased only at 72 h timepoint in parental cells and the number increased continuously in all timepoints in KO cells.

The nuclear signal intensity of pRPA increased only moderately with increasing MMC concentration in both cell lines (Figure 8A, B). The increase was not as clear as seen with yH2AX, for example. The results were inconclusive, and no clear trend with time could be observed.

A similar inconclusive trend was observed for 53BP1 signal intensity in both cell lines (Figure 9A, B). A slight decrease in intensity could be observed with longer timepoints. The maximum signal intensity did not increase when MMC concentration increased, and approximately similar levels of intensity were observed in both cell lines. Instead, the foci analysis yielded differences both with time, concentration and between cell lines. In parental cells, an increasing trend in nuclear foci number was observed with increased concentration of MMC (Figure 9C). Similarly, as with yH2AX staining, the foci number decreased after 8 h timepoint with lower concentration of MMC, whereas with 1000 nM MMC, foci number decreased only after 48 h timepoint in parental cells. In KO cells, 10 nM MMC already yielded the maximum number of observed foci and the highest concentration of MMC did not increase the foci number any further (Figure 9D).

With pKAP1 (Figure 10A, B) increase in nuclear signal intensity could only be observed at highest MMC concentration in both cell lines. after 24 h timepoint, the signal intensity started already to decrease in parental cells, but in KO cells, the trend in signal intensity was still increasing at the 72 h timepoint.

A change in RAD51 signal intensity was not observed in neither parental nor KO cell lines (Figure 11A, B). However, foci number increased as MMC concentration increased in parental cells (Figure 11C). With the two lowest concentrations of MMC after the 24 h timepoint the foci number started to decrease in parental cells. But with highest MMC concentration, an increasing number of foci was observed until the 48 h timepoint, and a

decrease was observed only at the 72 h timepoint. RAD51 is loaded to the DSB site by BRCA1 and BRCA2, and therefore, it was expected that the KO cells would not form foci in these conditions. Slight foci formation was visible in KO cells as well, but the foci number was significantly lower, and their appearance was less clear than in parental cells (Figure 11D).

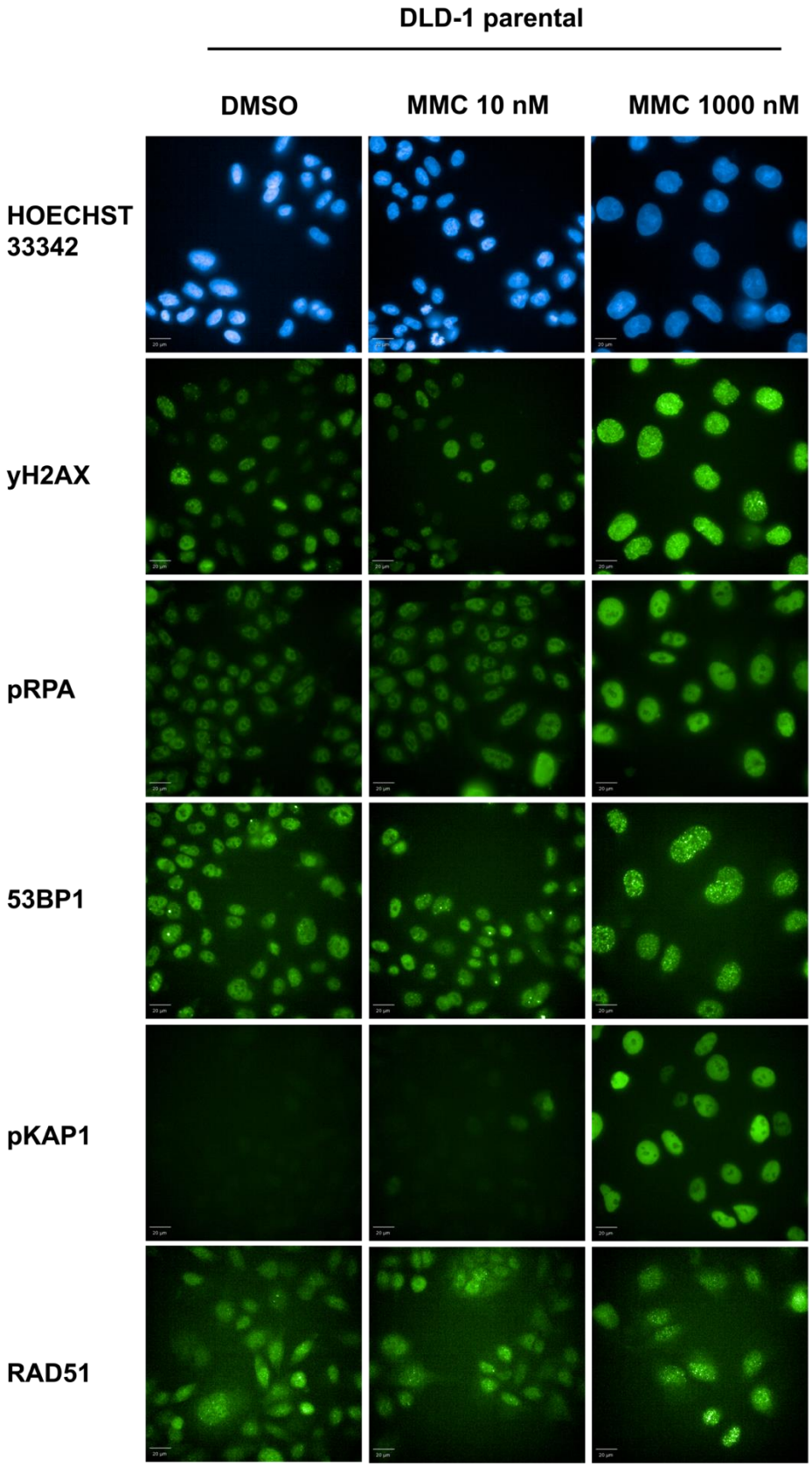

Figure 5. Representative immunofluorescence images of DLD-1 parental cells at 24 h timepoint after MMC 10 nM, MMC 1000 nM or DMSO treatment. Hoechst 33342 (blue) is used to stain nuclei, yH2AX, pRPA, 53BP1, pKAP1 and RAD51 are stained with Alexa Fluor 488 (green). Image parameters were determined for each antibody separately. Scalebar 20 µm.

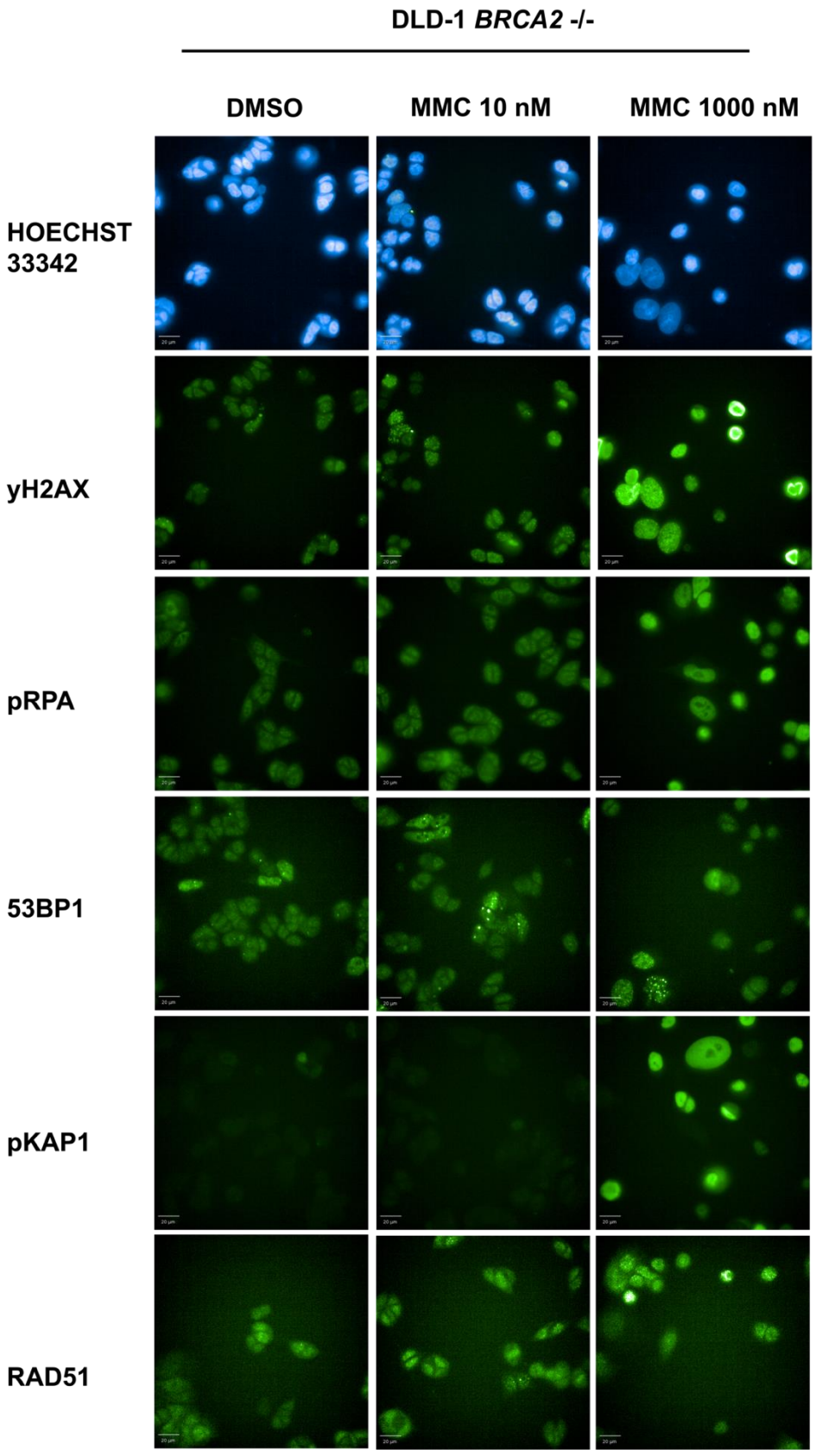

Figure 6. Representative immunofluorescence images of DLD-1 KO cells at 24 h timepoint after MMC 10 nM, MMC 1000 nM or DMSO treatment. Hoechst 33342 (blue) is used to stain nuclei, yH2AX, pRPA, 53BP1, pKAP1 and RAD51 are stained with Alexa Fluor 488 (green). Image parameters were determined for each antibody separately. Scalebar 20 µm.

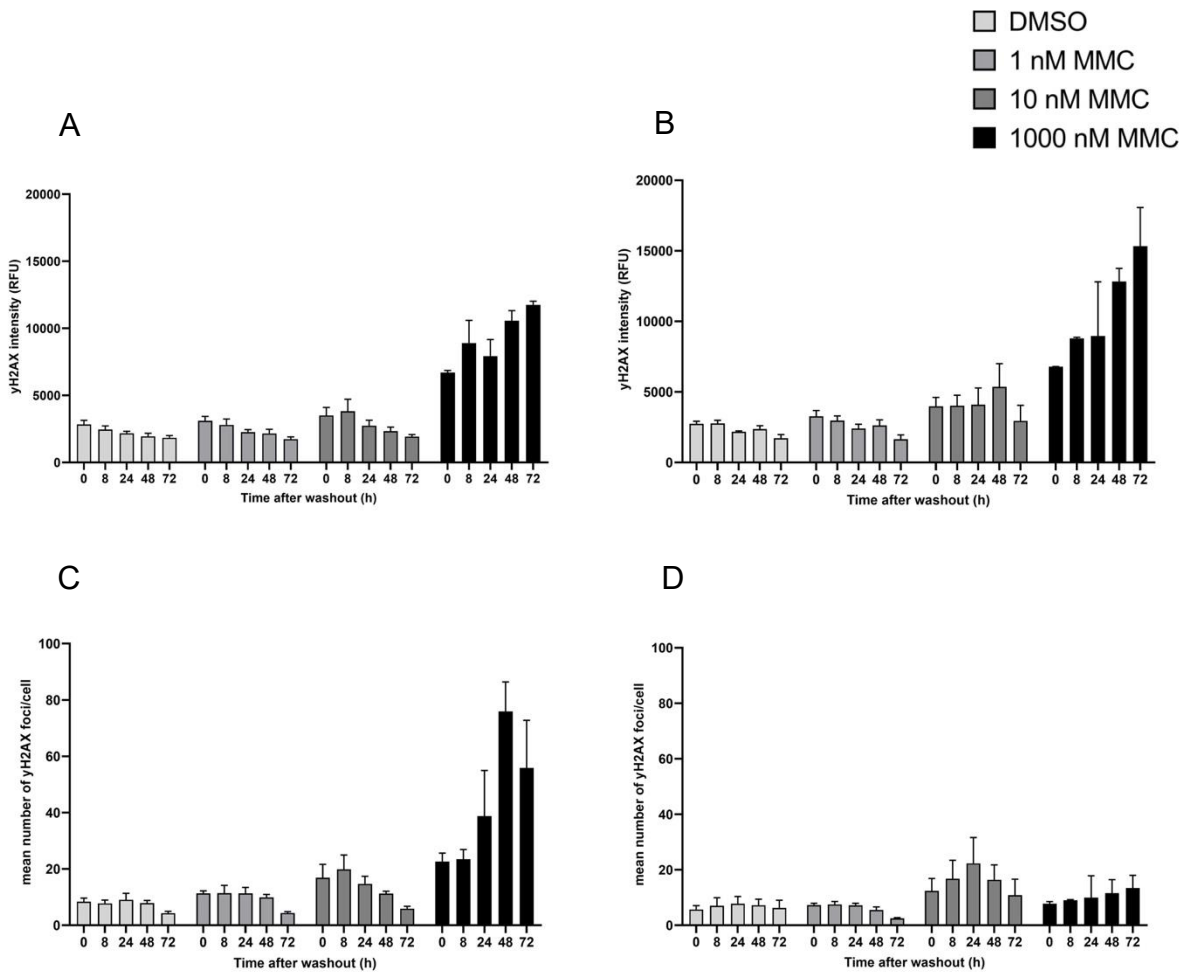

Figure 7. yH2AX signal intensity in (A) parental cells, (B) KO cells and mean number of foci per cell in (C) parental cells and (D) KO cells at different timepoints after MMC 1 nM, MMC 10 nM, MMC 1000 nM or DMSO treatment. Results represent the mean + SD, n = 3 experiments.

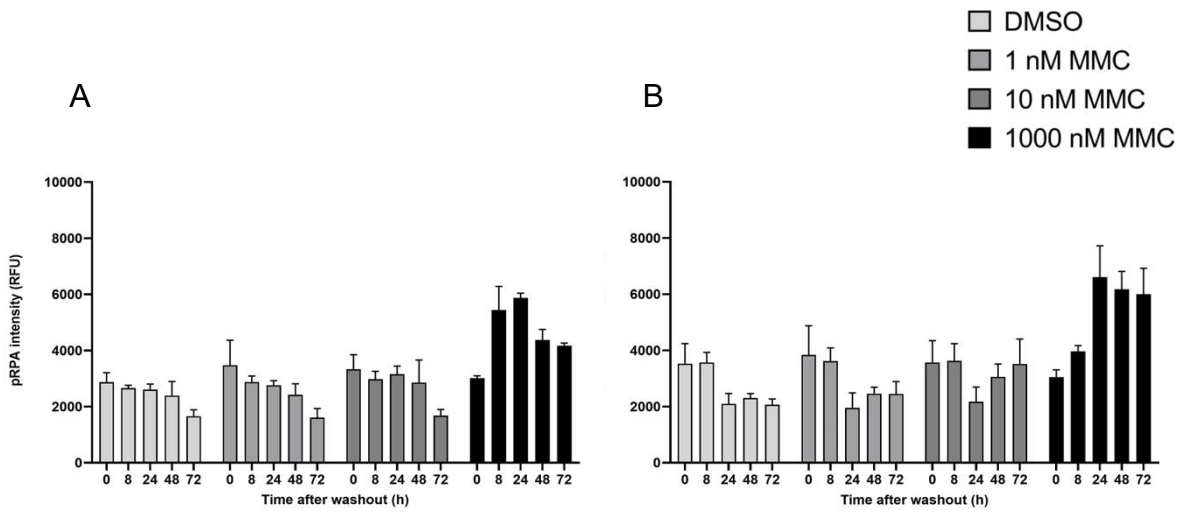

Figure 8. pRPA signal intensity in (A) parental cells and (B) KO cells at different timepoints after MMC 1 nM, MMC 10 nM, MMC 1000 nM or DMSO treatment. Results represent the mean + SD, n = 3 experiments.

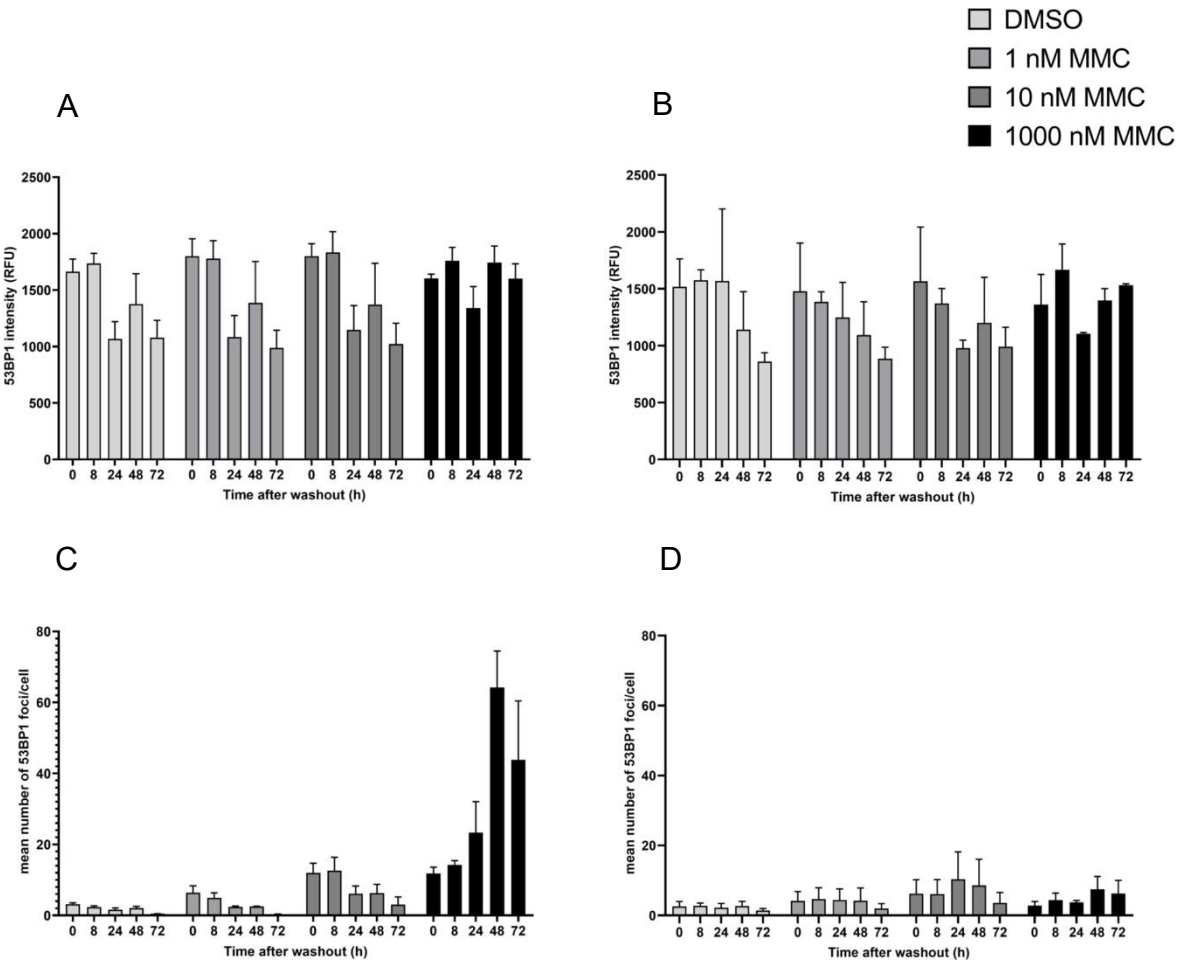

Figure 9. 53BP1 signal intensity in (A) parental cells and (B) KO cells and mean number of foci per cell in (C) parental cells and (D) KO cells at different timepoints after MMC 1 nM, MMC 10 nM, MMC 1000 nM or DMSO treatment. Results represent the mean + SD, n = 3 experiments.

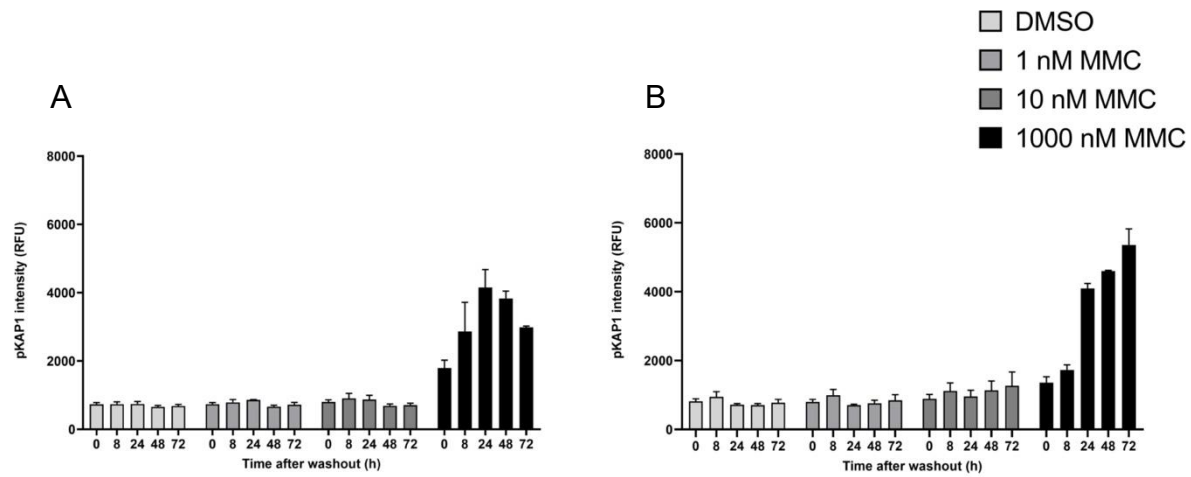

Figure 10. pKAP1 signal intensity in (A) parental cells and (B) KO cells at different timepoints after MMC 1 nM, MMC 10 nM, MMC 1000 nM or DMSO treatment. Results represent the mean + SD, n = 3 experiments.

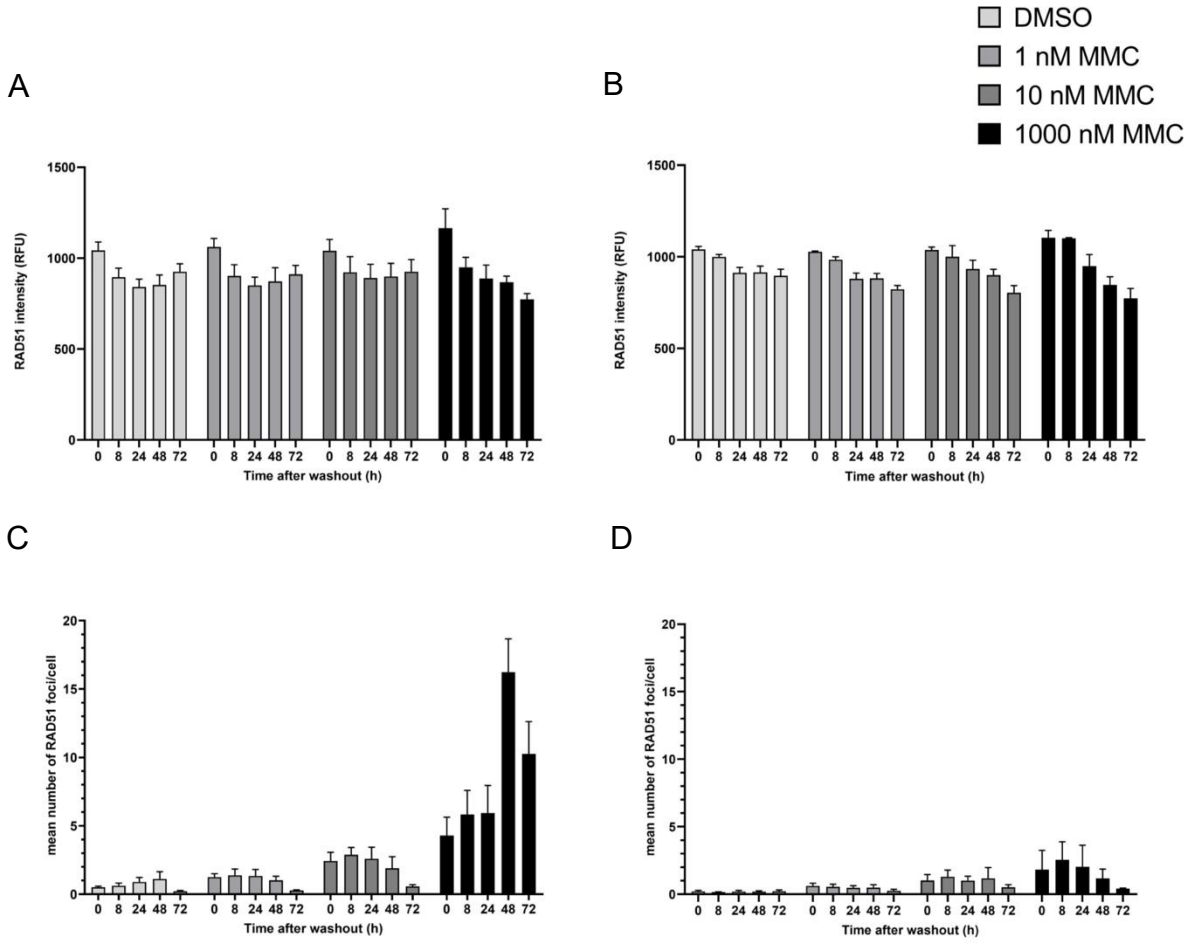

Figure 11. RAD51 signal intensity in (A) parental cells and (B) KO cells and mean number of foci per cell in (C) parental cells and (D) KO cells at different timepoints after MMC 1 nM, MMC 10 nM, MMC 1000 nM or DMSO treatment. Results represent the mean + SD, n = 3 experiments.

To study whether the expression and dynamics of the DNA damage markers change after treatment with targeted therapeutics, cells were treated with 100 nM or 1000 nM of ATR inhibitors ceralasertib, elimusertib and PARP inhibitors olaparib, veliparib and rucaparib for 24 h, 48 h or 72 h. To visualize the changes in markers, representative immunofluorescence images from all markers at 48 h timepoint after treatment with 100 nM compound are shown in Figures 12 and 13. As previously, image parameters were determined for each marker separately and intensities cannot be compared between different markers.

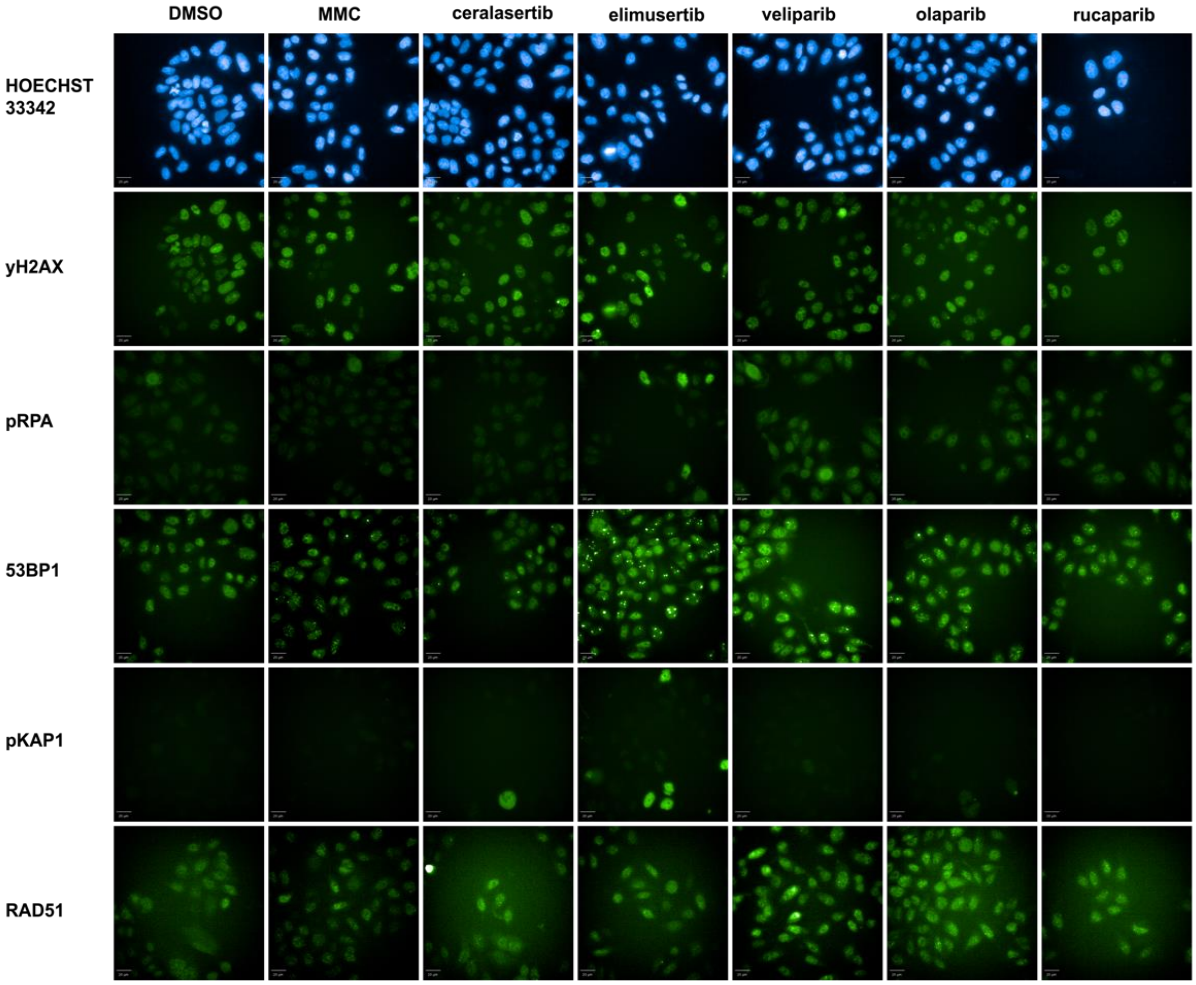

Figure 12. Representative immunofluorescence images of DLD-1 parental cells at 48 h timepoint after 100nM ATRi and PARPi treatments. Hoechst 33342 (blue) is used to stain nuclei, yH2AX, pRPA, 53BP1, pKAP1 and RAD51 are stained with Alexa Fluor 488 (green) Image parameters were determined for each antibody separately. Scalebar 20 µm.

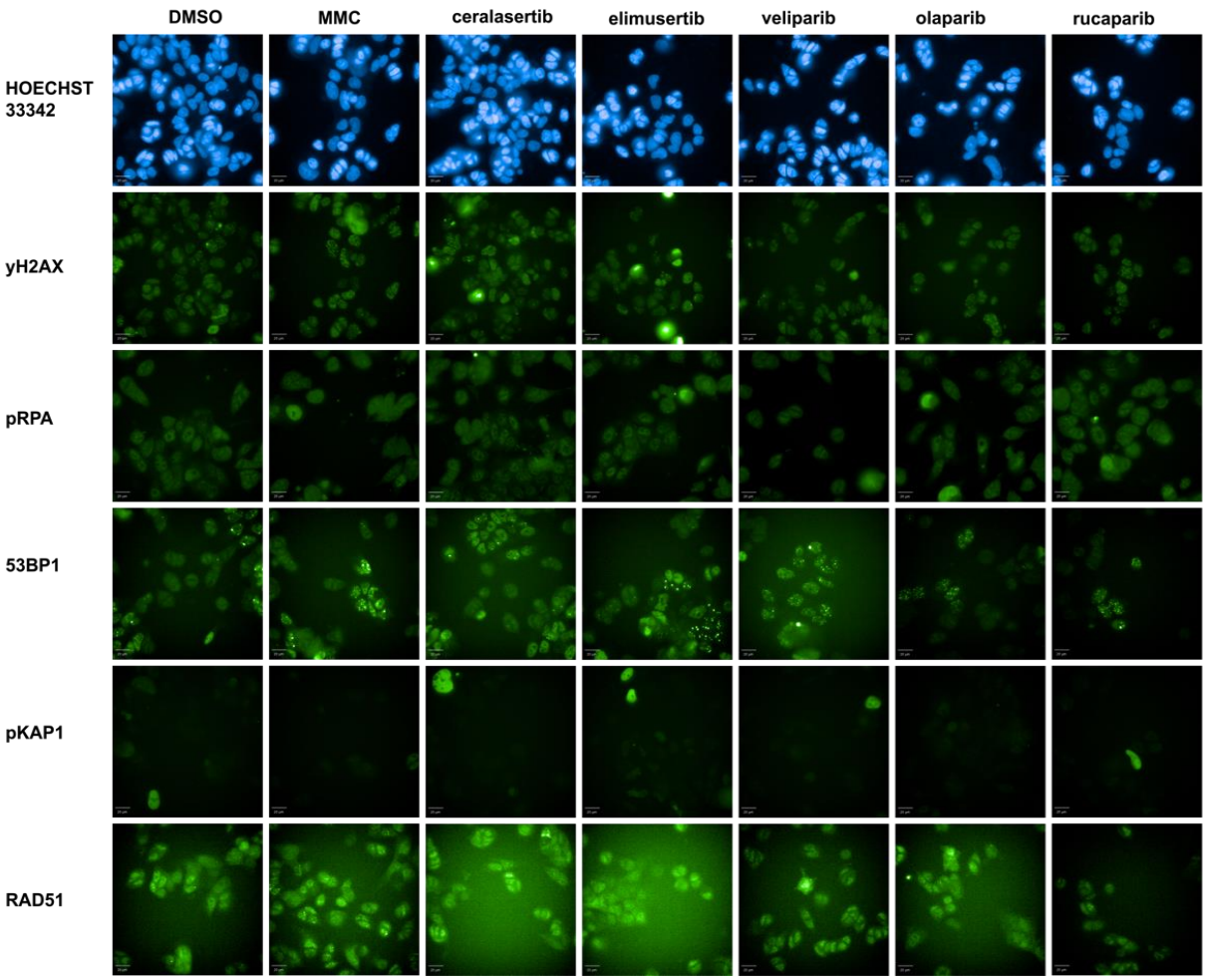

Figure 13. Representative immunofluorescence images of DLD-1 KO cells at 48 h timepoint after 100nM ATRi and PARPi treatments. Hoechst 33342 (blue) is used to stain nuclei, yH2AX, pRPA, 53BP1, pKAP1 and RAD51 are stained with Alexa Fluor 488 (green) Image parameters were determined for each antibody separately. Scalebar 20 µm.

No obvious changes could be observed visually form the images. Nuclear fluorescence signal intensity and mean nuclear foci number per cell were quantified from the images (Figures 14 – 18). Similar increase in the nuclei size that was noted in previous experiments, was not observed (Appendix 2). Only elimusertib increased yH2AX signal intensity, in both cell lines (Figure 14A, B). A quite clear dose-response could be observed with elimusertib, and the signal intensity increased at later timepoints. With other compounds, no induction of yH2AX signal was observed. yH2AX foci formation differentiated between compounds and between cell lines (Figure 14C, D). In both cell lines ATR inhibitors decreased the foci number, whereas PARP inhibitors increased the foci number as did MMC. In KO cells the differences between compounds were clearer than in parental cells. Within PARP inhibitors, a slight

difference could be noted as well. Olaparib and rucaparib seemed to increase the foci formation more than veliparib in KO cells at the 24 h and 48 h timepoint.

Nuclear signal intensity from pRPA increased only with elimusertib treatment (Figure 15A, B). With other compounds the intensity levels stayed quite steady, especially in KO cells.

Similar trend in signal intensity was present in 53BP1 as with MMC treatment. No clear dose-dependent induction, only modest increase in signal intensity by time could be observed (Figure 16A, B). However, more changes were observed in nuclear foci formation as was with yH2AX (Figure 16C, D). Especially PARP inhibitors increased the foci number, more in KO cells than in parental cells. There were also differences between PARP inhibitors, veliparib was clearly less potent of the three drugs to increase the foci number in KO cells.

pKAP1 signal intensity only increased with ATR inhibitors and clear dose-response to elimusertib at 24 h and 48 h timepoints could be observed in KO cells. In parental cells also ceralasertib increased the nuclear signal intensity at 72 h timepoint with 100 nM concentration. (Figure 17A, B).

With RAD51, no change in nuclear signal intensity was present (Figure 18A, B). In parental cells only MMC increased the foci formation (Figure 18C). In KO cells no clear foci formation was observed (Figure 18D). However, in all the timepoints, the signal intensity and foci number also increased in DMSO group with time. For this reason, these results are not unambiguous.

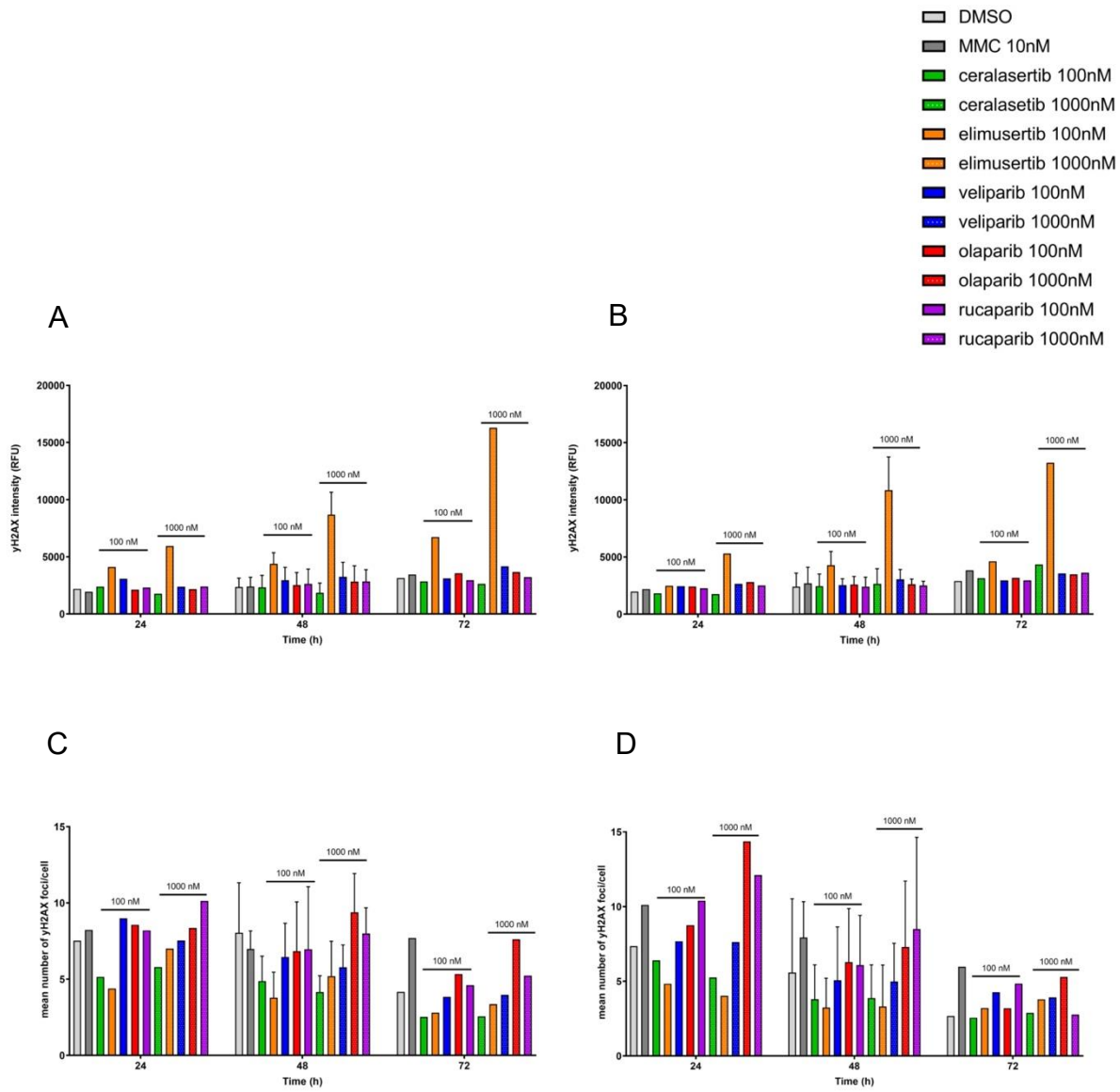

Figure 14. yH2AX signal intensity in (A) parental cells and (B) KO cells and mean number of foci per cell in (C) parental cells and (D) KO cells after 100 nM and 1000 nM ATRi and PARPi treatments for 24 h, 48 h or 72 h. Results represent the mean + SD. At 48 h timepoint n = 2 experiments, in other timepoints results represent mean on individual experiments.

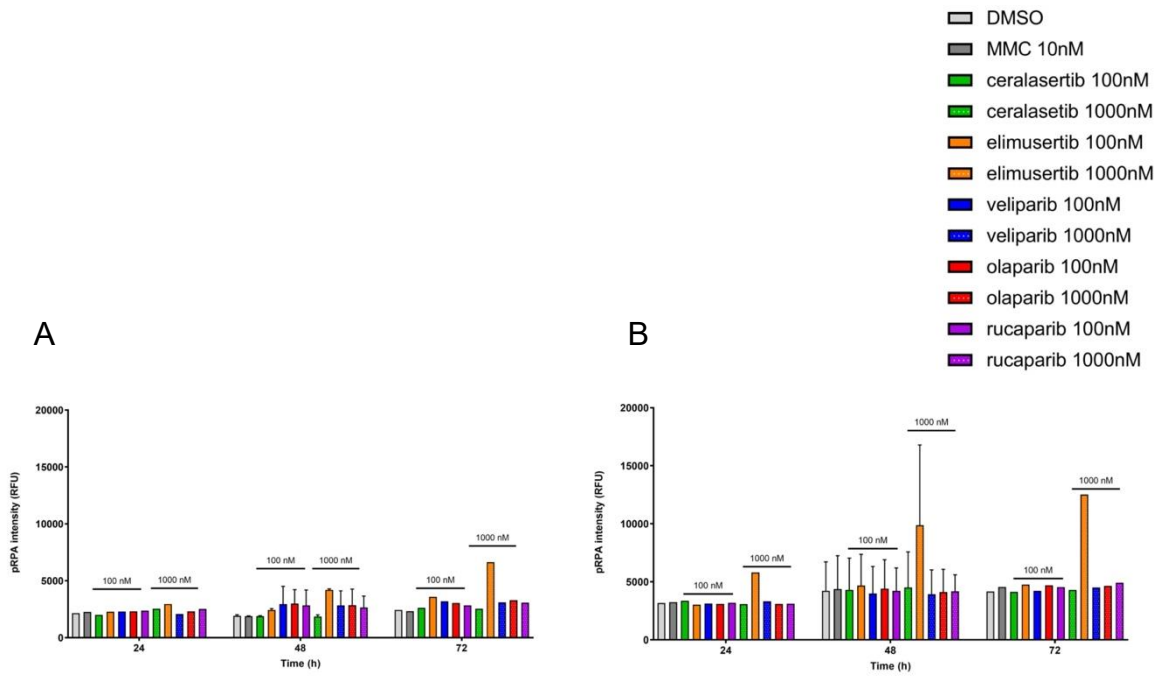

Figure 15. pRPA signal intensity (A) parental cells and (B) KO cells after 100 nM and 1000 nM ATRi and PARPi treatments for 24 h, 48 h or 72 h. Results represent the mean + SD. At 48 h timepoint n = 2 experiments, in other timepoints results represent mean on individual experiments.

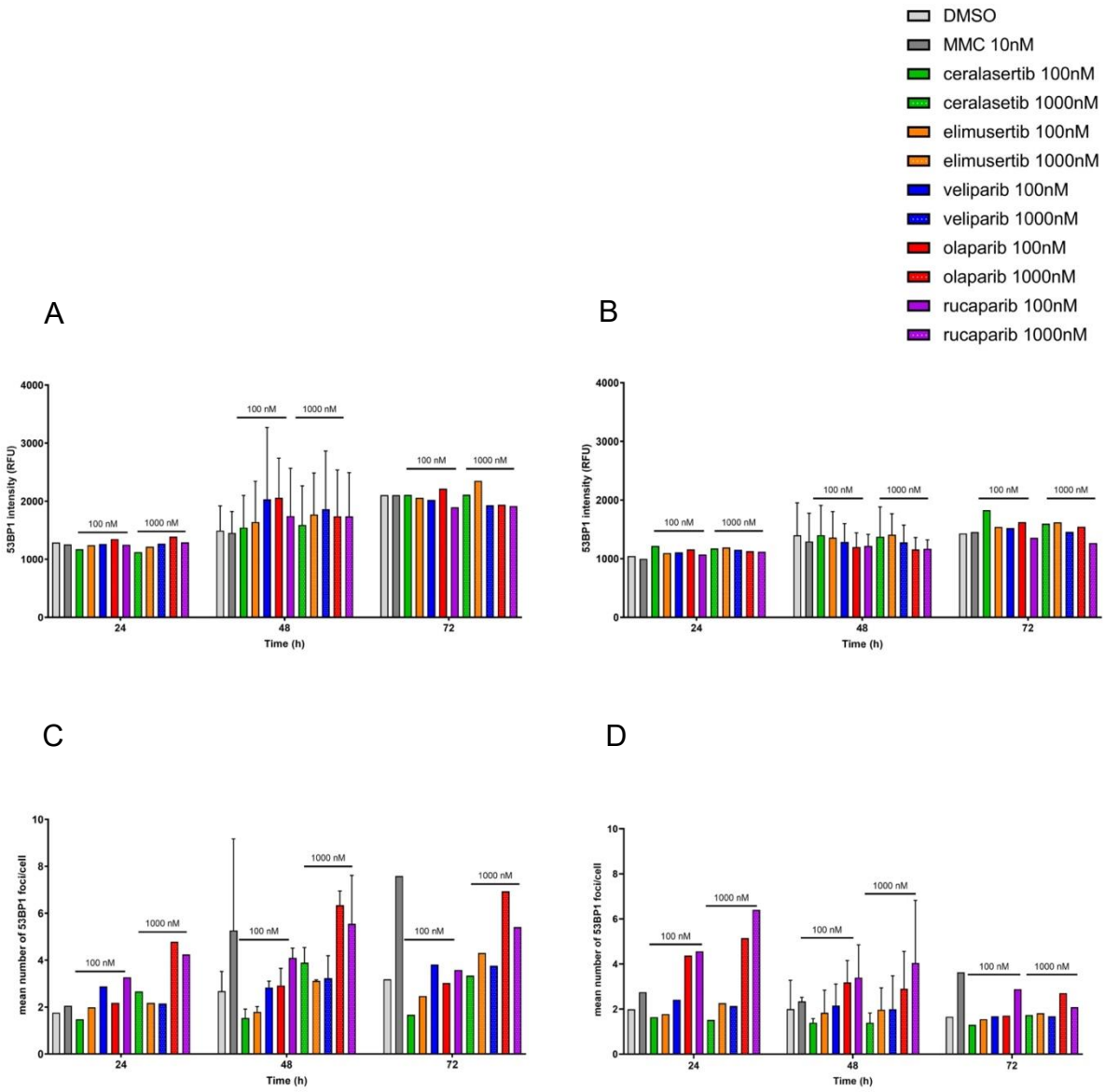

Figure 16. 53BP1 signal intensity in (A) parental cells and (B) KO cells and mean number of foci per cell in (C) parental cells and (D) KO cells after 100 nM and 1000 nM ATRi and PARPi treatments for 24 h, 48 h or 72 h. Results represent the mean + SD. At 48 h timepoint n = 2 experiments, in other timepoints results represent mean on individual experiments.

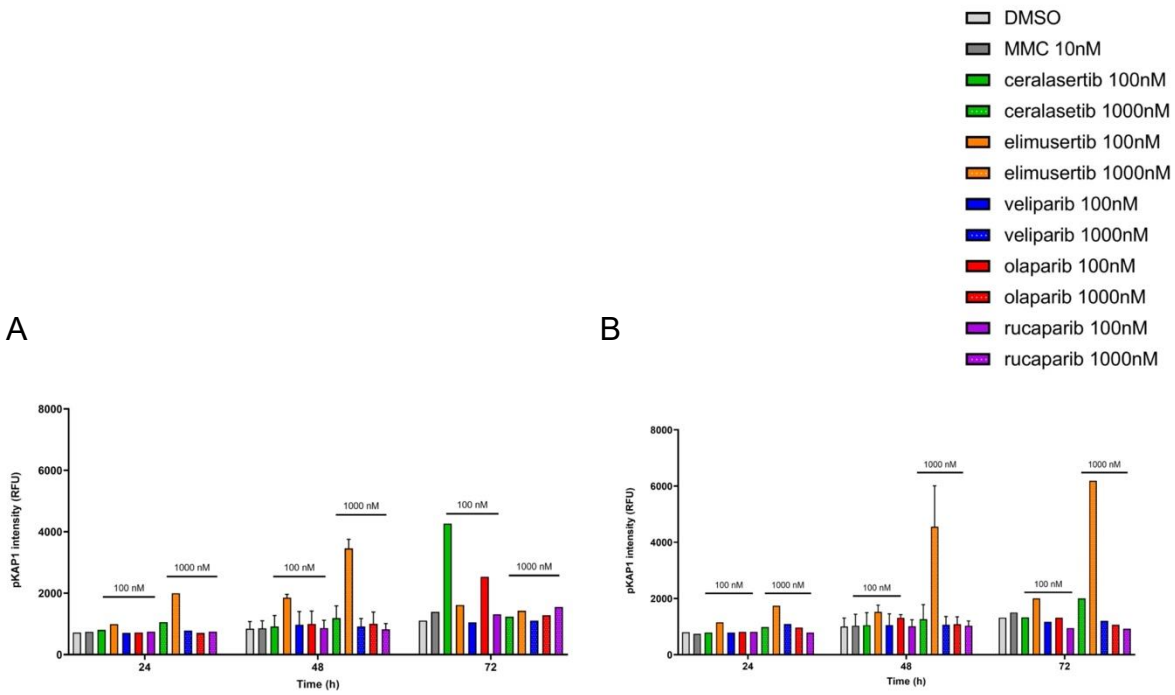

Figure 17. pKAP1 signal intensity (A) parental cells and (B) KO cells after 100 nM and 1000 nM ATRi and PARPi treatments for 24 h, 48 h or 72 h. Results represent the mean + SD. At 48 h timepoint n = 2 experiments, in other timepoints results represent mean on individual experiments.

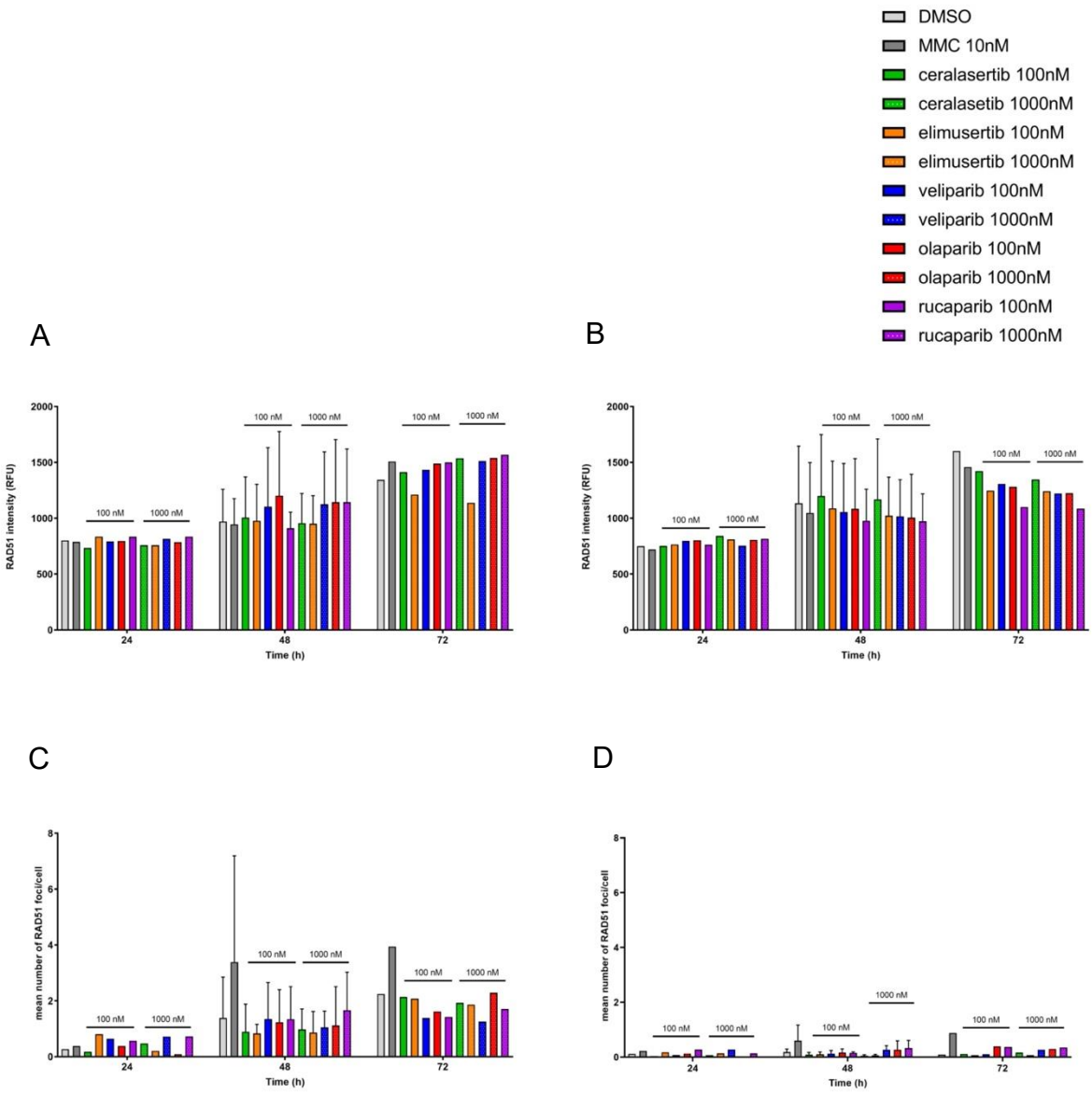

Figure 18. RAD51 signal intensity in (A) parental cells and (B) KO cells and mean number of foci per cell in (C) parental cells and (D) KO cells after 100 nM and 1000 nM ATRi and PARPi treatments for 24 h, 48 h or 72 h. Results represent the mean + SD. At 48 h timepoint n = 2 experiments, in other timepoints results represent mean on individual experiments.

2.4 Western blotting to observe changes at protein levels

To determine if the changes observed with immunofluorescence imaging could also be detected in total cell lysate western blotting was performed. Protein levels were studied after 6 h or 16 h treatment of 10 µM MMC. DMSO was used as negative control and vinculin as a loading control (Figure 19). pKAP1 signal was greatly increased after MMC treatments and

showed an increase by time as well. Modest increase in signal was observed also with pRPA at the 16 h treatment of MMC. RAD51 showed no differences neither in signal nor between cell lines. Signal from yH2AX slightly increased with longer treatment of MMC.

Similarly, as in immunofluorescence imaging, cells were also treated with 1000 nM ATR and PARP inhibitors for 72 h, and protein levels were compared with western blotting (Figure 20). Treatment with elimusertib dramatically increased the pKAP1 signal in both cell lines, whereas ceralasertib increased pKAP1 signal only little. Elimusertib also increased the signal of pRPA, RAD51 and yH2AX in parental cells. In KO cells almost no signal from RAD51 could be observed.

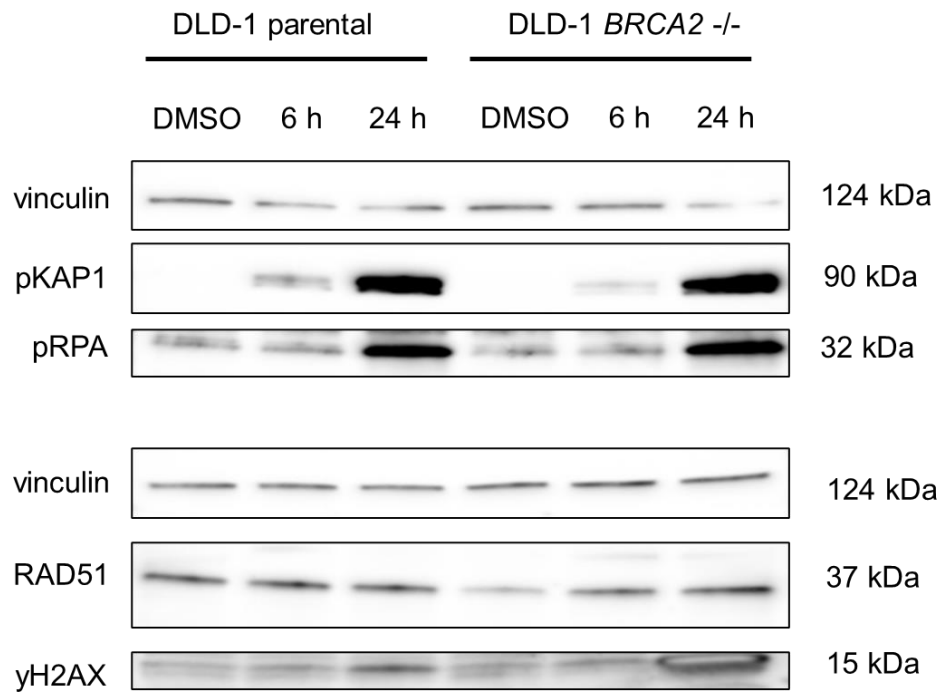

Figure 19. Western blot of protein samples from DLD-1 parental and KO after DMSO or 10 µM MMC treatment for 6 h or 24 h. Vinculin was used as loading control. The molecular weight (kDA) of each protein is presented on the right.

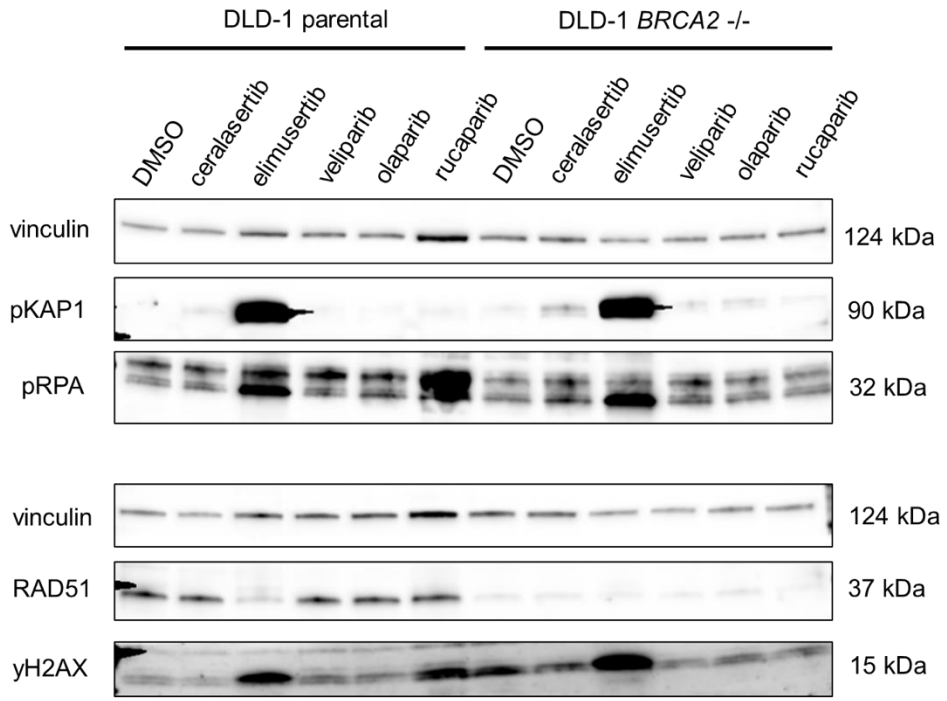

Figure 20. Western blot of protein samples from DLD-1 parental and KO cells after DMSO, 1000 nM ATRi or PARPi treatment for 72 h. Vinculin was used as loading control. The molecular weight (kDA) of each protein is presented on the right.

3 Discussion

3.1 Optimization of experiment conditions

Before final experiments all different experimental conditions were optimized. Optimization of fixing protocol and both primary and secondary antibody concentrations resulted in good and representative immunofluorescence samples. However, further optimization of pre-extraction protocol could have been applied; As the region of interest was the nucleus of cells, washing out the cytoplasmic fraction with the pre-extraction step could have decreased the background signal even more. However, nuclear foci could have been visualized better. It has been shown in various previous studies, that pRPA and pKAP1 both can form nuclear foci after irradiation-induced DSB and after treatment with hydroxyurea (Balajee and Geard, 2004; Noon et al., 2010). This suggests that these study conditions might not have been optimal, as in this study only homogenous fluorescence signals of pRPA and pKAP1 were obtained from the nuclei after chemically induced DNA damage with mitomycin C.

Western blotting optimization was successful as well. The visualization of 53BP1, however, would have required more optimization since it has been detected using western blotting in work by others (Ward et al., 2003). For example, longer run time and wet transfer could have been considered because of the high molecular weight (450 kDa) of 53BP1. More specific antibody could have been found for pRPA during the optimizations to avoid the unspecific binding seen in these experiments as a double band (Figures 19 and 20).

3.2 Dose response assay

The proliferation assay was performed to determine IC50 values for each compound and to ensure the functional consequence of the *BRCA2* knockout. A clear response to PARP inhibitors was observed with KO cells compared to the parental cells, and this assay validated the use of this cell pair for the current study. This proliferation assay also turned out to be very important, as it was noted that the KO cells started to lose the PARP response after being 2 – 3 months in culture. This was a new observation and a very important issue to consider in future when working with these cells.

the proliferation assay also showed significant difference between the two ATR inhibitors' IC50 values. IC50 values of elimusertib were significantly lower than IC50 values of ceralasertib in both cells (Table 2). This can result in the highest concentration of elimusertib (1000 nM) used in these experiments perhaps being toxic even for the parental cells. This

proliferation offered valuable information about the suitable working concentrations of each compound. In addition, this also provided information about the efficacy of PARP inhibitors on these cells. This proliferation clearly proved veliparib to be the weakest of these tested PARP inhibitors. Whether it being a result of the weaker trapping potential (Hopkins et al., 2019) or something else, will be discussed later.

3.3 Expression and dynamics of DNA damage markers

To study the expression and dynamics of the DNA damage markers, cells were treated with MMC to chemically induce DSB. Cells were treated with DMSO, 1 nM MMC, 10 nM MMC or 1000 nM MMC for 16 h followed by a medium change. 16 h treatment was considered to be enough time to introduce DSBs to cells, but not enough to lead to cell death. To study whether the expression and dynamics of the DNA damage markers would change after treatment with targeted therapeutics, cells were treated with 100 nM or 1000 nM of ATR inhibitors ceralasertib, elimusertib and PARP inhibitors olaparib, veliparib and rucaparib for 24 h, 48 h or 72 h. The concentrations were chosen based on the determined IC50 values of these compounds.

To ensure that the chemically induced DNA damage really resulted in DSBs, performing a DNA damage assay, such as comet assay, would have been useful. The comet assay would have shown the damage at single cell level and the degree of SSBs and DSBs. Also as stated in (Balajee and Geard, 2004), with comet assay even the correlation of foci formation and DSB repair could have been detected. Unfortunately, the planned experiments with comet assay for this study couldn’t be performed as missing components from the comet assay kit didn’t arrive in time for this thesis project.

Also, the induction of DSBs with irradiation would have been the optimal method, and that have been used in many previous studies on these DNA damage markers. With irradiation, controlled DSBs could have been induced and dose-response would have been perhaps more clearly observed. IR is a direct DNA damaging agent that causes multiple forms of DNA damage. It creates SSBs that can further develop into DSBs and DSBs directly. The dose of irradiation and thus the damage induced in cells is also adjustable and the beam of irradiation can be targeted accurately.

3.3.1 yH2AX

H2AX is phosphorylated at the damage site by ATM and ATR. The main function of yH2AX is thought to be the attraction of other repair proteins to the damage site (Kinner et al., 2008). yH2AX is considered as universal DNA damage marker (Cruz et al., 2018).

With 1 nM and 10 nM MMC, the foci number in parental cells clearly decreases at later timepoints already at 24 h (Figure 7), suggesting that the DSBs are being repaired and the DNA damage in cells decreases. In KO cells, however, the decrease is visible only at 48 h timepoint. At the highest MMC concentration in KO cells, 1000 nM, the peak in foci formation is at 48h timepoint whereas in KO cells, a slightly increasing trend can be observed still at 72 h timepoint. What should be noted is that with the 1000 nM MMC at 72 h timepoint the KO cells do not survive anymore (Appendix 1). In those conditions KO cells cannot proliferate anymore. In KO cells this can be observed as significantly bright nuclei with yH2AX staining, leading to that single foci are impossible to visualize, and therefore, leading to a significant decrease in the foci number in the foci analysis.

After 24 h a significant increase in nuclear size in parental cells was noted, in KO cell only modest increase (Appendix 1). Especially with yH2AX, the increase in the nuclei size, detected after 24 h post wash out with 1000 nM MMC treatment seems to affect the results. The foci number significantly increases as the nuclei size increases. Also, the foci appearance changes; they are smaller in size and brighter, increasing the total nuclei intensity signal as well. Also, the maximum of mean number of foci per cell was higher in parental cells, reaching approximately 80 foci/cell, whereas in KO cells, the maximum reached is approximately 25 foci/cell. This may be due to the repair efficiency or due to the nuclei size, which is being approximately 1,5 times larger in untreated cells and even up to 4 times larger in parental cells than in KO cells (Appendix 1.

After PARP inhibition, the number of yH2AX foci has been shown to increase (Cavallo et al., 2012) Also, after radiation-induced DSBs, it has been shown that the foci number increases (Ding et al., 2016). It was expected that treatment with ATRi and PARPi would have increased both the signal intensity and foci number significantly in both cell lines. This is the case especially in KO cells, where the SSBs induced by PARPi develop into DSBs when the cells replicate, and these DSBs cannot be repaired by HR due to the *BRCA2* mutation.

After PARPi and ATRi inhibition, a clear dose-dependent induction in yH2AX nuclear signal intensity was observed only with elimusertib (Figure 14). With none of the other used compounds no changes in signal intensity were observed. The increase with elimusertib only, and not with the other ATR inhibitor ceralasertib, might be due to the potency of elimusertib and it being potentially toxic to cells under these concentrations.

On the contrary to the expected results, in both cell lines, ATR inhibitors decreased the yH2AX foci number. PARP inhibitors modestly increased the foci number, as did MMC. In KO cells, the differences between PARPi were clearer than in parental cells. PARP inhibitors olaparib and rucaparib seemed to increase the foci formation more than veliparib. It could be speculated to be due to the PARP trapping potencies of the compounds. Veliparib is the weakest PARP trapper of these compounds, which could explain its higher IC50 value and lower number of foci formed (Murai et al., 2012). ATR inhibition did not increase the yH2AX foci formation probably because ATR inhibition alone does not directly induce DSBs. Rather the following inhibition of CHK1 leads to blockade of cell cycle checkpoints, leading to variety of different DNA damage in cells and ultimately to cell death.

What is important to keep in mind is that even though yH2AX is considered as a good and widely used marker of DNA damage, it is not only a DSB marker. In addition to DSBs, yH2AX foci can also increase due to stalled replication forks or in apoptosis (Löbrich et al., 2010). yH2AX foci can also appear at uncapped telomeres and during cellular senescence without the presence of DNA damage (Löbrich et al., 2010). In addition, genetic factors may influence the cells' ability to form yH2AX and to remove the phosphorylated residues after repair (Löbrich et al., 2010).

yH2AX could be considered rather an indirect marker of DSBs (Löbrich et al., 2010). Also, the timing of foci loss does not fully correlate with DSB repair. Currently, it is unclear whether loss of visible foci precisely correlates with the final step in the rejoining process or whether a delay of 1–2 h occurs, due to the additional time required to fully reconstitute the chromatin status (Löbrich et al., 2010).

3.3.2 pRPA

RPA binds to ssDNA, and in response to DNA damage, it is phosphorylated by ATM and ATR. It mediates the recruitment of other repair proteins, and it also prevents secondary structures of the ssDNA (Bhat and Cortez, 2018).

As mentioned earlier, pRPA has been shown to form quite clear foci. However, no clear foci were observed in this study. It was hypothesized that the signal intensity would increase with increased MMC concentration, but with the used concentrations, only modest increase was observed. When higher concentrations were used during the optimization with DMSO, 1 µM MMC and 10 µM MMC a clear induction in nuclear signal intensity was observed (data not shown). This indicates that an induction of pRPA in this experimental setting would require significantly higher concentrations of the damaging agent, MMC.

In previous studies, RPA foci is often presented instead of pRPA (Balajee and Geard, 2004). In these studies, a clear increase in the foci formation has been observed after irradiation (Balajee and Geard, 2004). The reason why only pan-nuclear staining of pRPA was observed in this study could be the timing. It may be that at the 0 h timepoint after MMC washout, phosphorylation has not yet been completed and that it has been lost at the 8 h timepoint.

ATR inhibition was expected to decrease the RPA phosphorylation, as its phosphorylation is partially mediated by ATR (Wang et al., 2001). In this study, an increase in the signal intensity was observed after treatment with the ATRi, elimusertib. However, it has been studied that only the inhibition of both ATM and ATR kinases completely prevents RPA foci formation (Block, Yu and Lees-Miller, 2004). The fact that multiple kinases regulate RPA phosphorylation, suggests that it has a crucial role in the DNA damage response (Block, Yu and Lees-Miller, 2004). This may explain why decrease in the signal intensity was not observed even with the highest concentration of elimusertib.

3.3.3 53BP1

53BP1 is a chromatin binding protein and it has a critical role in choosing the DSB repair pathway. It promotes repair by NHEJ pathway by antagonizing the end-resection needed for HR (Daley and Sung, 2014). It has been shown before that 53BP1 foci positively correlate with the IR dose and exhibit a linear dose-response relationship presenting DNA damage (Ding et al., 2016).

After MMC, ATRi and PARPi treatments, 53BP1 foci formation seems to follow a similar pattern as yH2AX. This may be expected as their co-localization has been studied and shown in previous research (Noon et al., 2010; Baldock et al., 2015; Ding et al., 2016). In addition, similar increase in foci formation as with yH2AX after treatment with olaparib and rucaparib, but less with veliparib, was observed. This may be a consequence of the IC50 value of

veliparib being a lot higher than IC50 values of olaparib and rucaparib. Meaning that a higher dose of veliparib would have needed to induce similar degree of damage to the cells as was induced with olaparib and rucaparib.

Visually the change in 53BP1 foci appearance is quite distinct as well. Cells treated with DMSO or 10 nM MMC have single bright foci, which are quite large. After 1000 nM MMC treatment the foci size decreases significantly in both cell lines. Also, even as the foci number seems to decrease after elimusertib treatment, the foci that are formed are brighter and larger than with other compounds.

As was mentioned, 53BP1 expression and dynamics seem to follow the pattern of yH2AX. This suggests that maybe 53BP1 could also be used alone as a marker of DNA damage. The observed foci are bright and clear to quantify. The correlation to repair status would, however, require more data.

3.3.4 pKAP1

KAP1 is required for the induction of heterochromatin relaxation during DNA repair. In response to DNA damage, KAP1 is phosphorylated by ATM and ATR which leads to local heterochromatin relaxation, giving access to the repair proteins to accumulate to the damage site (White et al., 2012).

In this study, induction in pKAP1 signal was only observed with MMC concentrations of 1 µM and above (data not shown). This suggests that only concentrations of MMC leading to cell death or causing severe cell stress are inducing pKAP1 expression. With concentrations that allowed the cells to proliferate normally and recover from the damage, induction of signal wasn't observed at any timepoint. (Hu et al., 2012) have shown that pKAP1 is linked to stress response after DNA damage, which could explain why a clear induction in signal intensity was observed only with high concentrations of MMC.

It was hypothesized that the inhibition of ATR would decrease the KAP1 phosphorylation and decrease the signal intensity. However, a complete opposite event was observed in this study; the only compound clearly inducing the pKAP1 signal was the ATR inhibitor elimusertib. The other ATR inhibitor ceralasertib only modestly induced the signal.

It has been shown that after DSB induction KAP1 is phosphorylated at Ser 824 by ATM (Noon et al., 2010). However, also phosphorylation at Ser 473 by ATM has been shown (Hu

et al., 2012). pKAP1 foci formation and a positive correlation to a cumulative dose of radiation has been shown (Noon et al., 2010; Hu et al., 2012; Ding et al., 2016). Complementary roles of ATM and ATR in KAP1 phosphorylation has been shown as well (Weber and Ryan, 2015). Inhibition of ATM or ATR alone did not decrease the foci formation but the inhibition of both did decrease the pKAP1 foci number (White et al., 2012). This may explain why the inhibition of ATR clearly increases the signal in this study as complementary roles and functional overlap between ATM and ATR have been shown (Cliby et al., 1998; Weber and Ryan, 2015).

As was mentioned earlier, it has been shown in many studies that pKAP1 does form nuclear foci, whereas in this study, only homogenous signal was observed in the nucleus (Noon et al., 2010; Ding et al., 2016). Before DSB, KAP1 exists in heterochromatin but after DSB induction, it is phosphorylated by ATM and it should result in formation of pKAP1 foci at damage sites (Noon et al., 2010; Ding et al., 2016) Antibodies recognizing both phosphorylation sites have been shown to detect the formed foci, although (White et al., 2012) state that S473p does not form foci but rather is diffusely located in the nucleus, while S824p does form foci. Whichever the case really is, the antibody that was used in this study recognizes the S824p site, suggesting that probably the reason for the lack of foci in this study might be because of timing rather than because of the used antibody. Even though (Noon et al., 2010) have shown pKAP1 foci even up to 24 h after IR, (Ziv et al., 2006) previously stated that after phosphorylation pKAP1 spread throughout nucleus, reaching pan-nuclear localization already within 15 minutes after IR. In addition to timing the used cell line, the damaging agents and the immunostaining protocol could have affected this as well.

3.3.5 RAD51

RAD51 replaces RPA on ssDNA at the damage site. It is loaded to the damage site by BRCA1 and BRCA2 (Laurini et al., 2020). This replacement of RPA with RAD51 is also the defining step of HR, and after that, the repair is committed to HR (Prakash et al., 2015).

Results of this study suggested that the nuclear intensity of RAD51 did not show any dose-response to MMC, ATRi or PARPi, nor did it change during different timepoints. At all timepoints and with both cell lines, the signal intensity increased in the DMSO group with time equally as after ATRi and PARPi treatment, suggesting that the observed slight increase is not a repair-related increase in signal intensity, but rather an increase caused by technical elements of the imaging.

Differences in RAD51 foci formation was clear between the cell lines. In parental cells, a clear dose-response and increase by time was observed after MMC, whereas in KO cells this cannot be seen. the results remain inconclusive after ATR and PARP inhibitor treatment. There aren´t clear differences between any of the compounds, except MMC, which increases RAD51 foci formation. However, as the KO cells started to lose the PARP response during the last repetitions in this study, some RAD51 foci formation was noticed during imaging after PARPi and ATRi treatment, especially at the 72 h timepoint. This suggests that KO cells started to restore the HR pathway with some unknown mechanisms or due to some new mutations.

These results suggest that RAD51 worked as was hypothesized; RAD51 formed nuclear foci in parental cells, whereas these foci did not form in KO cells. Thus, this suggests that RAD51 can be used as marker for functional HR as has been showed previously as well (Cruz et al., 2018). The lack of foci in KO cells, presented the status of HRD due to the *BRCA2* mutation. The later induction of RAD51 foci in KO cells would also suggest that RAD51 is quite good marker to PARP response.

In a study by (Cruz et al., 2018), the detection of RAD51 foci correlated with PARPi resistance in germline *BRCA1* mutated patient derived tumour xenografts. This suggests that RAD51 foci can be used as a biomarker also in clinics to better select patients for PARPi therapy (Cruz et al., 2018).

3.4. Western blot to observe changes from total cell lysates

Western blotting was performed after MMC, ATRi and PARPi treatments to study whether the changes observed with immunofluorescence imaging could be detected at protein level dynamics as well.

Clear changes in protein levels were detected with pKAP1 after both MMC and ATRi treatments. Similarly, ATRi increased pRPA protein levels and yH2AX levels. With MMC treatments, a modest increase in yH2AX protein levels was observed. yH2AX expression after 1 µM MMC and ATR inhibition is quite well in line with the results obtained from immunofluorescence imaging. Probably the DMSO sample from KO cells does not represent the actual biological response to DMSO but rather a technical error. yH2AX is known to be quite challenging phospho-protein to blot, as are generally all phospho-proteins. There is quite high risk that the phosphorylation can be lost during the cell lysis and handling of the

samples. In addition the molecular weight of yH2AX is very low (15 kDa) making it hard to detect with traditional western blot.

pRPA results were difficult to analyze as well. The true band of pRPA is likely the lower band of the visualized double-band. This band shows some response to the treatments, but it is not a clear result to draw any conclusion of. The increased expression of pKAP1 after 1 μM MMC and ATR inhibition is in line with the results obtained from immunofluorescence imaging.

The results of RAD51 protein expression are not clear. The differences between the two blots (Figures 19 and 20) were not expected. After MMC treatments no decrease in the RAD51 signal can be observed in the KO samples (Figure 19), however a clear decrease can be observed after ATRi and PARPi treatment (Figure 20). Rather than this overall increase or decrease in RAD51 amount, only localization to damage site would have been expected. The MMC treated samples (Figure 19) were later realized to be collected from KO cells that had already lost their PARPi response. However, this raises a question why treatment with elimusertib decreases the RAD51 signal in western blot samples but not in immunofluorescence samples. To deduce the real result, these western blots should be repeated with new samples from cells that with confirmed PARPi response.

Overall, the dynamics of these markers is difficult to compare with western blotting. Even though some changes were observed, and they supported the changes observed with immunofluorescence imaging, western blot cannot really be used as a single assay to study the DSB repair. In most of the previous studies of these DNA damage markers, western blotting is used to confirm the results from immunofluorescence imaging. And as with immunofluorescence imaging localization of proteins and their co-localizations with other proteins can be studied, western blot is performed to check the expression of a particular protein in cells or tissues. Performing both assays gives more reliability to the final conclusions and provides more support for new findings if designed well.

3.5 Study limitations

In addition to suggested modifications mentioned earlier, addition of other controls would have possibly supported these finding. To mention few: cell cycle checkpoint, RPA, KAP1, ATM/pATM, ATR/pATR in addition to cell cycle and apoptosis markers, could have been added. Especially the cell cycle markers would have been beneficial as it greatly affects the

marker dynamics and the initiation and timing of DSB repair. For example, in S phase, a high number of yH2AX foci can sometimes be seen without any obvious DNA damage (Kinner et al., 2008). Also, ATR can be activated in S-phase due to endogenous lesions or regions that are difficult to replicate, leading to ATR-dependent increase in yH2AX expression (Löbrich et al., 2010).

In image analysis the concept of foci analysis is ambiguous. In different studies, different number of foci is considered as threshold. A threshold for a foci-positive cell is in some studies more than 5 foci, in others more than 10, or in some studies certain percentage over baseline is considered positive (Roques et al., 2009). In some studies, a similar foci analysis as in this study has been applied: the mean number of foci/cell (Noon et al., 2010; Baldock et al., 2015). This analysis does not add an artificial threshold to the analysis, but it does have confounding factors; it overlooks the differences between cells. As in the heterogenic population of cells, some cells might have five foci, whereas some cells might have over 20 foci, resulting in the mean number of foci being 12 foci, which no longer represent neither of the cells. Foci properties could be measured as well. Foci size and brightness seems to change as well and could be analyzed. As each of these methods have their advantages and disadvantages, no one right method for foci quantification can be stated.

Also, the co-localization of foci might aid in the analysis, as it has been shown that many of these markers co-localize, better presenting the real DSB sites (White et al., 2012). Co-localization of yH2AX, 53BP1 and pKAP1 and pRPA has been shown (Balajee and Geard, 2004; White et al., 2012). Combination of several markers would also be better as analyzing the dynamics of only single marker could lead to wrong conclusion because of wrong timepoint, for example.

To be able to conclude the results form experiments with ATR and PARP inhibitors they should have been repeated still at least two more times. Due to time limitations different timepoints (24 h, 48 h and 72 h) had different number of repetitions, and there was quite high variation between samples. Also, in these experiments MMC, which was used as a positive control, should have been used with higher concentration for it to really work as a control. Now it behaved in similar manner as in previous experiments, but at the used timepoints (24 h, 48 h and 72 h) with the used concentration (10 nM) the yH2AX nuclear intensity signal levels, for example, had already decreased to the same level as in DMSO treated cells.

Similarly, as with IF imaging, additional controls could have been added to western blot as well to better analyze for example the ratio of phosphorylated protein and non-phosphorylated protein. Also, the interactions of the proteins cannot really be studied using western blot. The greatest limitation for western blot is obviously the specificity and availability of the used antibodies. Without good antibodies, the visualized bands can give false results. Also, western blot is rather non-quantitative method. Although the band intensities can be quantified and compared, the amount of protein present cannot be quantified.

Even though MMC did work in these experiments and did induce damage to cells, it does not represent all DSBs. MMC is an alkylating agent that inhibits DNA synthesis by cross-linking DNA strands of the DNA double helix (Crooke and Bradner, 1976). Additionally other DSB inducing agents could have been tried as well; Replication inhibitor hydroxyurea or other crosslinker cisplatin could have been tested. Also there are radiomimetic drugs, bleomycin for example, that imitate the effects of ionizing radiation that could have been tested as well (Vítor et al., 2020).

In addition to fluorescence signal intensity and foci formation, micronuclei formation could have been quantified from the immunofluorescence images. Micronuclei formation has been shown to be a quite reliable indicator for chromosome breakage and loss resulting from deficient DSB repair (Balajee and Geard, 2004; Fenech et al., 2020).

3.6 Conclusions

In this project, the aim was to find the best biomarker or biomarkers, and the best analysis method that could be used for drug discovery and development purposes.

Main findings of this study were that especially yH2AX and RAD51, which have been extensively described in literature, worked in these experiments as they were expected to behave, supporting their use as a biomarker of DNA damage and as a functional marker of HR. yH2AX nuclear signal intensity increase was observed with high concentrations of damaging agent, and it could be used to observe DNA damage in a robust manner. The foci analysis, however, shows more differences when working with lower concentrations and would detect smaller changes in the cells' response.

53BP1 followed yH2AX pattern. Only the foci analysis would be beneficial to use. Based on these experiments with pRPA and pKAP1 clearly the only method to analyze them are the differences in the nuclear signal intensity. For RAD51 in turn, the only working method is

foci analysis. pRPA and pKAP1 signals were only induced with µM concentrations of MMC and no foci formation was observed. However, with the higher concentrations clear increase in nuclear signal intensity was observed. This suggests that both could be potentially used as positive controls when studying DNA damage levels. 53BP1 foci formation did increase as the DNA damage increased. It may be used to simply determine the damage levels in cells. However, the differences between parental and KO cell lines, and therefore differences between cells with working HR and HRD cells should be further observed. RAD51 could be used in these experimental conditions as marker representing the HR status of the cells.

When considering the need for these markers to work in high-throughput assays, imaging with 63x objective is not convenient as it is quite time-consuming and less cells can be visualized in one field. 20x objective would be more optimal in timewise but with it all foci cannot be visualized; only yH2AX and 53BP1 foci were visualized, RAD51 foci was not. Next a 40x objective should be tested.

To choose which of the markers would be the best biomarker depends on the goal of the assay. If the purpose is to determine DNA damage, yH2AX foci and 53BP1 foci number could be applied. But it should be noted that yH2AX and 53BP1 foci can indicate DSB but not each focus truly represents a DSB. If working with high concentrations of damaging agents then the increase in yH2AX, pRPA and pKAP1 signal could be used. If being more interested in the HR status of the cells or screening responsive cell line to specific treatments, RAD51 foci formation would be the optimal choice.

To conclude, the results suggest that these proteins can be used as DNA damage biomarkers, but their wider use would still require further optimization. Depending on the goal, different marker will be optimal. Additionally, other cell lines should be added to the study as well, to observe whether these results could be applied generally.

4 Materials and methods

4.1 Cell maintenance and subculture

Cancer cells used in this project were obtained from Horizon Discoveries. The two used cell lines were DLD-1 parental (parental cells) (Horizon Discoveries PAR-008) and DLD-1 *BRCA2 -/-* (KO cells) (Horizon Discoveries 105-007), which are both colorectal adenocarcinoma Dukes Type C – cells. DLD-1 *BRCA2 -/-* cells are derived from the parental cell line and have a homozygous knockout of *BRCA2*.

Both cell lines were grown in RPMI 1640 medium with GlutaMAX supplement, supplemented with 10 % fetal bovine serum (FBS) and Penicillin-Streptomycin (10,000 U/mL, Pen Strep). Cells were grown at 37 °C with 5% carbon dioxide in a humified incubator. Cells were cultured as monolayer and passaged every 3 – 4 days when 70 – 80 % confluent. DLD-1 parental cells were split 1:10 – 1:20 and DLD-1 *BRCA2 -/-* cell approximately 1:3 – 1:6. For subculturing, confluent cell flasks were washed with 1x DPBS (Dulbecco's phosphate-buffered saline) and incubated with 0.25% Trypsin until cells were detached. Culture medium was used to inactivate trypsin and cells were centrifuged (800 rpm, 5 min, RT). Cells were re-seeded in culture medium to Nunc T75 culture flasks. Details of the materials used in cell culture are presented in Table 3.

Table 3. Materials used in cell culture.

Material	Supplier	Catalog number
DPBS (Dulbecco's phosphate buffered saline)	Gibco ThermoFisher Scientific	14190-094
Trypsin (0.5% Trypsin- EDTA)	Gibco ThermoFisher Scientific	15400-054
RPMI 1640 Medium, GlutaMAX Supplement	Gibco ThermoFisher Scientific	61870-010
FBS	Sigma-Aldrich	F7524
Pen Strep	Gibco ThermoFisher Scientific	15140-122
Nunc EasyFlask 75cm2 Nunclon Delta Surface	ThermoFisher Scientific	156499

4.2 Dose response assay

A six-day proliferation assay was performed to observe the cells' response to PARP inhibitors, ATR inhibitors and MMC. DLD-1 parental and KO cells were plated on Poly-D lysine (PDL)-coated CellCarrier Ultra 384-well microplates (PerkinElmer, 6057302). A serial dilution curve from 10 µM with 3.162 dilution factor was used with all compounds. 0.1 % DMSO and 10 µM MMC were used as controls. Compounds are listed in Table 4. After six days, plates were fixed with 3.7 % formaldehyde solution (Sigma-Aldrich, 252549) in PBS with Hoechst 33342 for 15 minutes at room temperature and washed with DBPS. After fixing, plates were imaged with Operetta CLS (PerkinElmer) with Harmony software (PerkinElmer, 4.9.2137.273). A 10x air objective was used to image nuclei. The images were exported, and nuclear fluorescence intensity signal and foci formation were analyzed with Columbus (Columbus, 2.9.1. 146585, PerkinElmer). IC50 values were calculated in GraphPad Prism.

Table 4. Compounds used in proliferation assay

Compound	Class	Supplier	Cat. No.
Mitomycin C	DNA crosslinker	MedChem Express	HY-13316
Olaparib	PARPi	MedChem Express	HY-10162
Rucaparib	PARPi	MedChem Express	HY-10617A
Veliparib	PARPi	MedChem Express	HY-10129
Ceralasertib (AZD6738)	ATRi	MedChem Express	HY-19323
Elimusertib (BAY 1895344)	ATRi	MedChem Express	HY-101566

4.3 Immunofluorescence imaging

4.3.1 Antibody optimization for immunostaining

Primary antibodies were first optimized for immunofluorescence imaging. Parental cells were plated on Poly-D lysine (PDL)-coated CellCarrier Ultra 96-well microplates (PerkinElmer, 6055500). The following day, cells were treated with either 0.3 % DMSO (Sigma-Aldrich, D2650) or 10 µM mitomycin c (MMC) for 6 h. Cells were then fixed either with 3.7 % formaldehyde solution (Sigma-Aldrich, 252549) in PBS for 15 minutes at room temperature or with ice cold 100 % methanol for 10 min in room temperature. Cells were washed with DPBS, and last, left in DBPS and stored at +4 °C if not continued immediately with the staining protocol.

After fixing, cells were washed with 0.2 % Triton™ X-100 (Sigma-Aldrich, X100) in DPBS (PBST) and blocked for 1 hour at room temperature (RT) with 5 % BSA (Sigma-Aldrich, A2153) in 0.2 % PBST. After blocking, cells were incubated with primary antibodies diluted in 5 % BSA in PBST overnight at +4 °C. Cells were washed with 5 % BSA in DPBS and incubated with secondary antibodies diluted in 5 % BSA in DPBS for 1 hour, in dark, RT. After incubation, cells were washed with 5 % BSA in DPBS and with DPBS. Last, cells were left in DPBS, and the plate was imaged with 63x water objective with Operetta CLS (PerkinElmer) with the Harmony software (PerkinElmer, 4.9.2137.273). The images were exported and analyzed using Columbus (Columbus, 2.9.1. 146585, PerkinElmer). See table 5 for antibodies and dilutions tested.

Secondary antibodies are needed to provide the detectable signal of the target protein where the primary antibody has been bound. Due to high background signal obtained from secondary antibody, they were optimized as well. Parental and KO cells were treated as previously, fixed as described earlier, stained with yH2AX primary antibody or BSA, and the following day, different concentrations of secondary antibodies were tested (Table 5).

4.3.2 Pre-extraction

To better visualize the nuclear proteins and the nuclear foci, a pre-extraction protocol was applied to the staining protocol. Parental cells were treated with MMC as previously. Before fixing the pre-extraction was performed. Wells were washed with DPBS and incubated on ice for 10 min in pre-extraction buffer (0.5 % Triton-X-100, 20 mM Hepes (pH 7.4), 50 mM NaCl, 3 mM MgCl2, 300 mM sucrose), and last, washed with cold DPBS. Standard fixation with PFA or methanol was followed, and plates were imaged as before.

Table 5. Antibodies and dilutions tested in optimization

	Supplier name/Target	Supplier	Catalog number	Dilution in immunofluorescence imaging
Primary antibodies				
	Phospho-Histone H2A.X (Ser139)	Cell Signaling	#9718	1:400; 1:1200; 1:3600
	Phospho-RPA32 (S4/S8)	Bethyl Laboratories	IHC-00422	1:50; 1:150; 1:450

	Supplier name/Target	Supplier	Catalog number	Dilution in immunofluorescence imaging
	Phospho-RPA32/RPA2 (Ser8)	Cell Signaling	#54762	1:200; 1:600; 1:1800
	53BP1	Cell Signaling	#4937	1:100; 1:300; 1:900
	Phosphor KAP-1 (S824)	Bethyl Laboratories	A700-013	1:100; 1:300; 1:900
	Rad51	Cell Signaling	#8875	1:100; 1:300; 1:900
Secondary antibodies				
	Goat anti-rabbit IgG Alexa 488	LifeTechnologies	A11034	1:500; 1:1000; 1:2000
	Goat anti-rabbit IgG Alexa 568	LifeTechnologies	A11011	1:500; 1:1000; 1:2000
	Hoechst 33342	Life Technologies	H3570	1:10.000

4.3.3 Optimization of MMC-treatment conditions

Different timepoints and different concentrations were tested for MMC. First, cells were treated with 10 µM MMC for three different timepoints: 30 h, 22 h and 6 h. Also, longer timepoints were tested with different concentrations of MMC; 1 µM and 10 µM of MMC were tested at 2 h, 6 h, 16 h, 24 h, 48 h, 72 h, 96 h. Cells were treated with MMC as described before, and fixing and staining protocol was applied.

Next a washout step was added to optimizations to allow the cells to repair the damage and proliferate. Cells were treated with 10 µM or 1 µM MMC for 16 h, fresh culture medium was changed to all wells and plates were fixed 0 h, 8 h, 24 h, 48 h and 72 h after washout.

To final experiments using MMC, same protocol with washout step was applied. Final antibodies and dilutions are presented in Table 6.

4.3.4 ATRi and PARPi experiments

To study the changes in markers after treatment with PARP and ATR inhibitors, parental and KO cells were plated to Poly-D lysine (PDL)-coated CellCarrier Ultra 384-well microplates (PerkinElmer, 6057302) in which the compounds had already been dispensed using Echo® 655 liquid handling system (Labcyte). Compounds were added in two different concentrations

100 nM and 1000 nM, based on the IC50 values obtained earlier (Table 2). 10 nM MMC and 0.1 % DMSO were added as controls. Cells were treated for 24 h and 48 h or 48 h and 72 h, after which plates were fixed and stained as described earlier. Plates were imaged with Operetta 63x water objective and analyzed in Columbus.

Table 6. Antibodies and dilutions used in immunofluorescence staining.

	Supplier name/Target name	Supplier	Catalog number	Dilution in immunofluorescence imaging
Primary antibodies				
	Phospho-Histone H2A.X (Ser139)	Cell Signaling	#9718	1:400
	Phospho-RPA32 (S4/S8)	Bethyl Laboratories	A300-245A	1:500
	Phospho-RPA32/RPA2 (Ser8)	Cell Signaling	#54762	1:200
	53BP1	Cell Signaling	#4937	1:100
	Phosphor KAP-1 (S824)	Bethyl Laboratories	A700-013	1:100
	Rad51	Cell Signaling	#8875	1:100
Secondary antibodies				
	Goat anti-rabbit IgG Alexa 488	LifeTechnologies	A11034	1:500
	Hoechst 33342	Life Technologies	H3570	1:10.000

4.4 Protein extraction, SDS-PAGE, and western blot analysis

For western blotting, parental and KO cells were plated in six well plates (Corning CellBIND, 3335) and treated for 72 h with 0,1 % DMSO, 1000 nM PARP inhibitors or 1000 nM ATR inhibitors. MMC samples were prepared in Nunc T25 culture flasks (ThermoFisher Scientific, 156340) and treated with 0.3 % DMSO or 10 µM MMC for 6 h or 16 h.

To extract proteins, samples were washed with PBS and lysed for 30 minutes in RIPA buffer (ThermoFisher, #89900) supplemented with 4% protease inhibitor solution (Complete EDTA-free, Roche, #11873580001 in Milli-Q) and 10 % phosphatase inhibitor solution (PhosSTOP,

Roche, #04906837001 in RIPA buffer). After lysis, samples were centrifuged 15 min at +4 °C 14,000x g. Supernatant was collected after centrifugation.

The protein concentration of the collected samples was determined using Micro BSA Protein Assay Kit (Thermo Scientific, #23235) according to the manufacturer's instructions. The luminescence was measured with EnSpire Microplate Reader 23001365 with software EnSpire 4.1.

Samples for western blotting were prepared on ice. Samples were diluted to the wanted concentration (20 ug protein/sample) with lysis buffer (TermoFisher Scientific, 78501) and 1x Laemmli (BioRad, 161-0747) supplemented with B-mercaptoethanol (Sigma, M3148). Laemmli is added the better isolate the proteins in SDS-PAGE gel electrophoresis. Samples were boiled 5 min at 95 °C, and rapidly centrifuged at 10,000 rpm. Samples were loaded to 4 – 15 % Criterion Stain Free TM Tris-HCL protein gel (BioRad, 567-8083). Precision Plus Protein WesternC Blotting Standard (BioRad, #1610376) was used as molecular weight standard. Tris/Glycine/SDS buffer (BioRad, #161-0772) was used as running buffer. Gel was run with 80 V – 120 V. During this SDS (sodium dodecyl sulfate–polyacrylamide) electrophoresis step proteins in the samples are separated based on size; Smaller proteins migrate easier through the gel than larger proteins, leading to the separation by size. The gradient gel was used to obtain better separation of proteins.

Next a transfer step was performed to transfer the proteins from gel to a solid membrane. Gel was transferred to Tris/Glycine -transfer buffer (BioRad, #1610734). Trans-BlotR Turbo TM Midi Nitrocellulose Transfer packs (BioRad, #1704159) and semi-dry transfer was used with the Tran-Blot Turbo MIXED MW program (2.5 A constant: up to 25 V, 7 min). After transfer, membranes were blocked for 1 hour at RT in EveryBlot Blocking Buffer (BioRad, #12010020). Blocking was performed to prevent non-specific binding of antibodies during next steps.

For primary antibodies, the membranes were incubated overnight at +4 °C on a shaker. Primary antibodies were non-labeled and bind directly to the target protein. Membranes were washed with 1xTBS Tween20 (TBST, ThermoFisher Scientific, 28360). After washing, membranes were incubated with secondary antibodies and Precision Protein StrepTactin-HRP conjugate 1:10,000 (BioRad, #161-0381) in blocking buffer for 1 hour at RT and after incubation washed with 1xTBST. Secondary antibodies that bind to the primary antibodies

are used to detect the proteins using chemiluminescence. Dilutions for primary and secondary antibodies that were tested are in Table 7 and final used antibodies and dilutions in Table 8.

For detection, Clarity Western ECL substrate (BioRad, #170-5061) was used to all antibodies except to yH2AX, for which Clarity Max Western ECL Substrate (BioRad, #1705062) was used. Both substrates were used according to the manufacturer's instructions. ECL is based on the reaction between the added ECL substrate and the HRP labeled antibodies. This reaction emits a chemiluminescence signal that can be detected by digital imaging system. Membranes were scanned with Azure c400 Gel imaging system cSeries Capture Software (1.9.2.0315) (Azure Biosystems).

Table 7. Antibodies and dilutions tested in optimization of Western Blot.

	Supplier name/Target	Supplier	Catalog number	Dilution in Western blot
Primary antibodies				
	Anti-phospho-Histone H2A.X (Ser139) Antibody, clone JBW301	Merck	05-636	1:1000
	Phospho-Histone H2A.X (Ser139) (20E3)	Cell Signaling	#9718	1:1000
	Phospho-RPA32 (S4/S8)	Bethyl Laboratories	IHC-00422	1:1000
	Phospho-RPA32/RPA2 (Ser8)	Cell Signaling	#54762	1:1000
	53BP1	Cell Signaling	#4937	1:1000
	Phosphor KAP-1 (S824)	Bethyl Laboratories	A700-013	1:1000
	Recombinant Anti-Rad51 antibody [EPR4030(3)]	Abcam	ab133534	1:1000
	Rad51 (D4B10)	Cell Signaling	#8875	1:1000
	Recombinant Anti-Vinculin	Abcam	ab129002	1:10,000

	Supplier name/Target	Supplier	Catalog number	Dilution in Western blot
	antibody [EPR8185]			
Secondary antibodies				
	Goat anti-rabbit IgG-HRP	BioRad	#1706515	1:3000
	Goat anti-mouse IgG-HRP	BioRad	#1706516	1:3000

Table 8. Final antibodies and dilutions used in western blotting.

	Supplier name/Target name	Supplier	Catalog number	Dilution in Western blot
Primary antibodies				
	Anti-phospho-Histone H2A.X (Ser139) Antibody, clone JBW301	Merck	05-636	1:750
	Phospho-RPA32 (S4/S8)	Bethyl Laboratories	A300-245A	1:2000
	Phosphor KAP-1 (S824)	Bethyl Laboratories	A700-013	1:1000
	Rad51	Cell Signaling	#8875	1:1000
	Recombinant Anti-Vinculin antibody [EPR8185]	Abcam	ab129002	1:10,000
Secondary antibodies				
	Goat anti-rabbit IgG-HRP	BioRad	#1706515	1:3000
	Goat anti-mouse IgG-HRP	BioRad	#1706516	1:3000

4.4.1 Data analysis

Data from Columbus was analyzed with GraphPad Prism Software (9.1.0 (221)). For IC50 value calculations, data was normalized to DMSO and MMC controls to obtain a range from 100 % to 0 % in relative viability. A non-linear regression was used to fit the dose-response curve.

4.4.2 Image analysis

All immunofluorescence images were analyzed with Columbus software (Columbus, 2.9.1. 146585, PerkinElmer). The pre-built analyses with adjusted parameters in Columbus were used. Image analysis was built by first defining nuclei in the images with HOECHST 33342 channel (Figure 21A). Only whole nuclei that were completely inside the image were chosen for the analysis. Nuclear intensity was calculated from the selected nuclear area from the Alexa Fluor 488 channel. For the foci analysis, a spot analysis inside the nucleus was built as well using the Alexa Fluor 488 channel (Figure 21B). Parameters for the analysis were adjusted for both cell lines, for each antibody and for each repetition as needed to obtain as representative segmentation as possible.

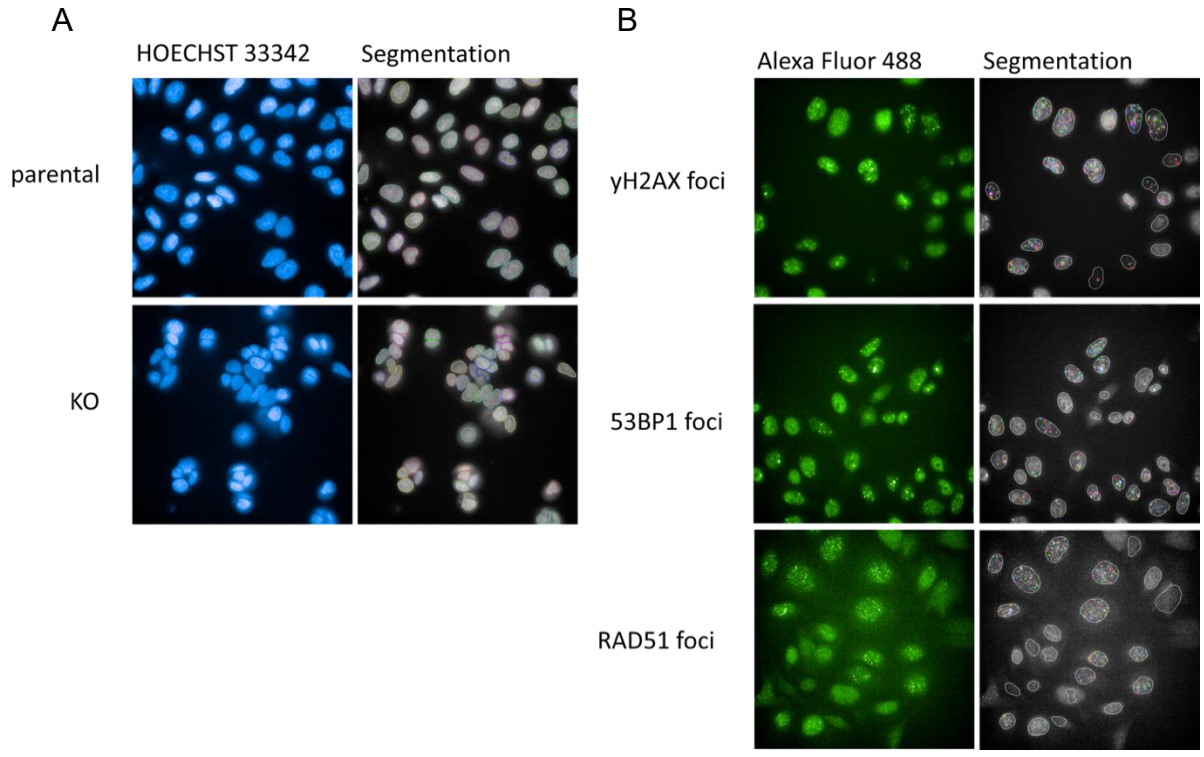

Figure 21. Image analysis was built with segmentation of (A) nucleus for intensity and segmentation of (B) foci for spot analysis in Columbus. Parameters for the analysis were adjusted for both cell lines and for each antibody as needed to obtain as representative segmentation as possible.

5. Acknowledgements

I would firstly like to especially thank my supervisors Julia Lindqvist and Johanna Ahlskog for always supporting me and being ready to answer my questions. Their true interest towards this project and their vivid conversations of the acquired results gave me a great perspective for this whole project. I also want to thank my other team members in Cancer Genomics team and other team members in Orion R&D who have helped me. A special thanks goes to Leena Kahala for helping me with everything regardless of the problem. I wouldn't have been able to carry out this whole project without all of you.

And of course, I want to thank my family and friends for always supporting me both in my studies throughout these years and through this project. I want to express my gratitude to my parents and grandparents for always being interested of my research and listening to me and asking questions. Thank you everyone.

Abbreviations

53BP1	Tumor suppressor P53-binding protein 1
ATM	ataxia telangiectasia mutated
ATR	ATM and Rad3-related
ATRi	ATM and Rad3-related inhibitor
Alt-EJ	Alternative end joining
BER	Base excision repair
BRCA1/2	Breast cancer susceptibility gene 1/2
CDK1/2	Cyclin-dependent kinase 1/2
CHK1/2	Checkpoint kinase 1/2
CtIP	CtBP-interacting protein
DDR	DNA damage response
DNA	deoxyribonucleic acid
DNA-PK	DNA-dependent protein kinase
DSB	double strand break
dsDNA	double strand DNA
yH2AX	gamma histone 2AX
HR	homologous recombination
HRD	homologous recombination deficient
IR	ionizing radiation
KAP1	Kruppel-associated box (KRAB)3-associated protein 1
MDC1	Mediator of DNA damage checkpoint protein 1
MMC	Mitomycin C

MMEJ	Microhomology-mediated end joining
MMR	mismatch repair
MSI	microsatellite instable
NER	Nucleotide excision repair
NHEJ	Non-homologous end joining
PARP	Poly (ADP-ribose) polymerase
PARPi	Poly (ADP-ribose) polymerase inhibitor
PDL	Poly-D lysine
PFA	paraformaldehyde
PIKKs	phosphatidylinositol 3-kinase-like protein kinases
RAD51	RAD51 homolog
ROS	reactive oxygen species
RPA	replication protein A
RT	room temperature
ssDNA	single strand DNA
SSA	Single strand annealing
UV	ultraviolet
WEE1	WEE1 G2 Checkpoint Kinase
XP	Xeroderma pigmentosum

References

de Almeida, L.C., Calil, F.A., Machado-Neto, J.A. and Costa-Lotufo, L.V., 2021. *DNA damaging agents and DNA repair: From carcinogenesis to cancer therapy*. *Cancer Genetics*, https://doi.org/10.1016/j.cancergen.2020.12.002.

Balajee, A.S. and Geard, C.R., 2004. Replication protein a and γ-H2AX foci assembly is triggered by cellular response to DNA double-strand breaks. *Experimental Cell Research*, 300(2). https://doi.org/10.1016/j.yexcr.2004.07.022.

Baldock, R.A.A., Day, M., Wilkinson, O.J.J., Cloney, R., Jeggo, P.A.A., Oliver, A.W.W., Watts, F.Z.Z. and Pearl, L.H.H., 2015. ATM Localization and Heterochromatin Repair Depend on Direct Interaction of the 53BP1-BRCT2 Domain with γH2AX. *Cell Reports*, 13(10). https://doi.org/10.1016/j.celrep.2015.10.074.

Barnieh, F.M., Loadman, P.M. and Falconer, R.A., 2021. Progress towards a clinically-successful ATR inhibitor for cancer therapy. *Current Research in Pharmacology and Drug Discovery*, 2. https://doi.org/10.1016/j.crphar.2021.100017.

Bhat, K.P. and Cortez, D., 2018. *RPA and RAD51: Fork reversal, fork protection, and genome stability*. *Nature Structural and Molecular Biology*, https://doi.org/10.1038/s41594-018-0075-z.

Block, W.D., Yu, Y. and Lees-Miller, S.P., 2004. Phosphatidyl inositol 3-kinase-like serine/threonine protein kinases (PIKKs) are required for DNA damage-induced phosphorylation of the 32 kDA subunit of replication protein A at threonine 21. *Nucleic Acids Research*, 32(3). https://doi.org/10.1093/nar/gkh265.

Bradbury, A., Hall, S., Curtin, N. and Drew, Y., 2020. *Targeting ATR as Cancer Therapy: A new era for synthetic lethality and synergistic combinations? Pharmacology and Therapeutics*, https://doi.org/10.1016/j.pharmthera.2019.107450.

Bridges, C.B., 1922. The Origin of Variations in Sexual and Sex-Limited Characters. *The American Naturalist*, 56(642). https://doi.org/10.1086/279847.

Brown, J.S., O'Carrigan, B., Jackson, S.P. and Yap, T.A., 2017. *Targeting DNA repair in cancer: Beyond PARP inhibitors*. *Cancer Discovery*, https://doi.org/10.1158/2159-8290.CD-16-0860.

Burma, S., Chen, B.P., Murphy, M., Kurimasa, A. and Chen, D.J., 2001. ATM Phosphorylates Histone H2AX in Response to DNA Double-strand Breaks. *Journal of Biological Chemistry*, 276(45). https://doi.org/10.1074/jbc.C100466200.

Byrne, B.M. and Oakley, G.G., 2019. *Replication protein A, the laxative that keeps DNA regular: The importance of RPA phosphorylation in maintaining genome stability*. *Seminars in Cell and Developmental Biology*, https://doi.org/10.1016/j.semcdb.2018.04.005.

Carrassa, L. and Damia, G., 2017. *DNA damage response inhibitors: Mechanisms and potential applications in cancer therapy*. *Cancer Treatment Reviews*, https://doi.org/10.1016/j.ctrv.2017.08.013.

Cavallo, F., Graziani, G., Antinozzi, C., Feldman, D.R., Houldsworth, J., Bosl, G.J., Chaganti, R.S.K., Moynahan, M.E., Jasin, M. and Barchi, M., 2012. Reduced Proficiency in Homologous Recombination Underlies the High Sensitivity of Embryonal Carcinoma

Testicular Germ Cell Tumors to Cisplatin and Poly (ADP-Ribose) Polymerase Inhibition. *PLoS ONE*, 7(12). https://doi.org/10.1371/journal.pone.0051563.

Ceccaldi, R., Rondinelli, B. and D'Andrea, A.D., 2016. *Repair Pathway Choices and Consequences at the Double-Strand Break. Trends in Cell Biology*, https://doi.org/10.1016/j.tcb.2015.07.009.

Chatterjee, N. and Walker, G.C., 2017. *Mechanisms of DNA damage, repair, and mutagenesis*. *Environmental and Molecular Mutagenesis*, https://doi.org/10.1002/em.22087.

Cheng, C.-T., 2014. KAPtain in charge of multiple missions: Emerging roles of KAP1. *World Journal of Biological Chemistry*, 5(3). https://doi.org/10.4331/wjbc.v5.i3.308.

Cleary, J.M., Aguirre, A.J., Shapiro, G.I. and D'Andrea, A.D., 2020. *Biomarker-Guided Development of DNA Repair Inhibitors*. *Molecular Cell*, https://doi.org/10.1016/j.molcel.2020.04.035.

Cliby, W.A., Roberts, C.J., Cimprich, K.A., Stringer, C.M., Lamb, J.R., Schreiber, S.L. and Friend, S.H., 1998. Overexpression of a kinase-inactive ATR protein causes sensitivity to DNA-damaging agents and defects in cell cycle checkpoints. *EMBO Journal*, 17(1). https://doi.org/10.1093/emboj/17.1.159.

Crooke, S.T. and Bradner, W.T., 1976. *Mitomycin C: a review*. *Cancer Treatment Reviews*, https://doi.org/10.1016/S0305-7372(76)80019-9.

Cruz, C., Castroviejo-Bermejo, M., Gutiérrez-Enríquez, S., Llop-Guevara, A., Ibrahim, Y.H., Gris-Oliver, A., Bonache, S., Morancho, B., Bruna, A., Rueda, O.M., Lai, Z., Polanska, U.M., Jones, G.N., Kristel, P., de Bustos, L., Guzman, M., Rodríguez, O., Grueso, J., Montalban, G., Caratú, G., Mancuso, F., Fasani, R., Jiménez, J., Howat, W.J., Dougherty, B., Vivancos, A., Nuciforo, P., Serres-Créixams, X., Rubio, I.T., Oaknin, A., Cadogan, E., Barrett, J.C., Caldas, C., Baselga, J., Saura, C., Cortés, J., Arribas, J., Jonkers, J., Díez, O., O'Connor, M.J., Balmaña, J. and Serra, V., 2018. RAD51 foci as a functional biomarker of homologous recombination repair and PARP inhibitor resistance in germline BRCA-mutated breast cancer. *Annals of Oncology*, 29(5). https://doi.org/10.1093/annonc/mdy099.

Curtin, N.J., 2012. *DNA repair dysregulation from cancer driver to therapeutic target*. *Nature Reviews Cancer*, https://doi.org/10.1038/nrc3399.

Daley, J.M. and Sung, P., 2014. 53BP1, BRCA1, and the Choice between Recombination and End Joining at DNA Double-Strand Breaks. *Molecular and Cellular Biology*, 34(8). https://doi.org/10.1128/mcb.01639-13.

Ding, D., Zhang, Y., Wang, J., Wang, X., Fan, D., He, L., Zhang, X., Gao, Y., Li, Q. and Chen, H., 2016. γ-H2AX/53BP1/pKAP-1 foci and their linear tracks induced by in vitro exposure to radon and its progeny in human peripheral blood lymphocytes. *Scientific Reports*, 6. https://doi.org/10.1038/srep38295.

Dobzhansky, T., 1946. Genetics of natural populations; recombination and variability in populations of Drosophila pseudoobscura. *Genetics*, 31. https://doi.org/10.1093/genetics/31.3.269.

Fenech, M., Knasmueller, S., Bolognesi, C., Holland, N., Bonassi, S. and Kirsch-Volders, M., 2020. *Micronuclei as biomarkers of DNA damage, aneuploidy, inducers of chromosomal hypermutation and as sources of pro-inflammatory DNA in humans*.

Mutation Research - Reviews in Mutation Research, https://doi.org/10.1016/j.mrrev.2020.108342.

Gou, R., Dong, H. and Lin, B., 2020. *Application and reflection of genomic scar assays in evaluating the efficacy of platinum salts and PARP inhibitors in cancer therapy*. *Life Sciences*, https://doi.org/10.1016/j.lfs.2020.118434.

Grundy, M.K., Buckanovich, R.J. and Bernstein, K.A., 2020. Regulation and pharmacological targeting of RAD51 in cancer. *NAR Cancer*, 2(3). https://doi.org/10.1093/narcan/zcaa024.

Gudmundsdottir, K. and Ashworth, A., 2006. *The roles of BRCA1 and BRCA2 and associated proteins in the maintenance of genomic stability*. *Oncogene*, https://doi.org/10.1038/sj.onc.1209874.

Ha, D.H., Min, A., Kim, S., Jang, H., Kim, S.H., Kim, H.J., Ryu, H.S., Ku, J.L., Lee, K.H. and Im, S.A., 2020. Antitumor effect of a WEE1 inhibitor and potentiation of olaparib sensitivity by DNA damage response modulation in triple-negative breast cancer. *Scientific Reports*, 10(1). https://doi.org/10.1038/s41598-020-66018-5.

Hanahan, D. and Weinberg, R.A., 2011. *Hallmarks of cancer: The next generation*. *Cell*, https://doi.org/10.1016/j.cell.2011.02.013.

Her, J. and Bunting, S.F., 2018. *How cells ensure correct repair of DNA double-strand breaks*. *Journal of Biological Chemistry*, https://doi.org/10.1074/jbc.TM118.000371.

Hoeijmakers, J.H.J., 2001. *Genome maintenance mechanisms for preventing cancer*. *Nature*, https://doi.org/10.1038/35077232.

Hopkins, T.A., Ainsworth, W.B., Ellis, P.A., Donawho, C.K., DiGiammarino, E.L., Panchal, S.C., Abraham, V.C., Algire, M.A., Shi, Y., Olson, A.M., Johnson, E.F., Wilsbacher, J.L. and Maag, D., 2019. PARP1 trapping by PARP inhibitors drives cytotoxicity in both cancer cells and healthy bone marrow. *Molecular Cancer Research*, 17(2). https://doi.org/10.1158/1541-7786.MCR-18-0138.

Hsieh, P. and Yamane, K., 2008. DNA mismatch repair: Molecular mechanism, cancer, and ageing. *Mechanisms of Ageing and Development*, 129(7–8). https://doi.org/10.1016/j.mad.2008.02.012.

Hu, C., Zhang, S., Gao, X., Gao, X., Xu, X., Lv, Y., Zhang, Y., Zhu, Z., Zhang, C., Li, Q., Wong, J., Cui, Y., Zhang, W., Ma, L. and Wang, C., 2012. Roles of Kruppel-associated box (KRAB)-associated co-repressor KAP1 Ser-473 phosphorylation in DNA damage response. *Journal of Biological Chemistry*, 287(23). https://doi.org/10.1074/jbc.M111.313262.

Jachimowicz, R.D., Goergens, J. and Reinhardt, H.C., 2019. *DNA double-strand break repair pathway choice - from basic biology to clinical exploitation*. *Cell Cycle*, https://doi.org/10.1080/15384101.2019.1618542.

Jalal, S., Earley, J.N. and Turchi, J.J., 2011. *DNA repair: From genome maintenance to biomarker and therapeutic target*. *Clinical Cancer Research*, https://doi.org/10.1158/1078-0432.CCR-11-0761.

Jang, S.M., Kauzlaric, A., Quivy, J.P., Pontis, J., Rauwel, B., Coluccio, A., Offner, S., Duc, J., Turelli, P., Almouzni, G. and Trono, D., 2018. KAP1 facilitates reinstatement of heterochromatin after DNA replication. *Nucleic Acids Research*, 46(17). https://doi.org/10.1093/nar/gky580.

Janysek, D.C., Kim, J., Duijf, P.H.G. and Dray, E., 2021. *Clinical use and mechanisms of resistance for PARP inhibitors in homologous recombination-deficient cancers*. *Translational Oncology*, https://doi.org/10.1016/j.tranon.2021.101012.

Kinner, A., Wu, W., Staudt, C. and Iliakis, G., 2008. *Gamma-H2AX in recognition and signaling of DNA double-strand breaks in the context of chromatin. Nucleic acids research*, https://doi.org/10.1093/nar/gkn550.

Klinakis, A., Karagiannis, D. and Rampias, T., 2020. *Targeting DNA repair in cancer: current state and novel approaches*. *Cellular and Molecular Life Sciences*, https://doi.org/10.1007/s00018-019-03299-8.

Laurini, E., Marson, D., Fermeglia, A., Aulic, S., Fermeglia, M. and Pricl, S., 2020. *Role of Rad51 and DNA repair in cancer: A molecular perspective*. *Pharmacology and Therapeutics*, https://doi.org/10.1016/j.pharmthera.2020.107492.

Lavin, M.F. and Yeo, A.J., 2020. *Clinical potential of ATM inhibitors*. *Mutation Research - Fundamental and Molecular Mechanisms of Mutagenesis*, https://doi.org/10.1016/j.mrfmmm.2020.111695.

Löbrich, M., Shibata, A., Beucher, A., Fisher, A., Ensminger, M., Goodarzi, A.A., Barton, O. and Jeggo, P.A., 2010. *γH2AX foci analysis for monitoring DNA double-strand break repair: Strengths, limitations and optimization*. *Cell Cycle*, https://doi.org/10.4161/cc.9.4.10764.

Lowndes, N.F. and Toh, G.W.L., 2005. *DNA repair: The importance of phosphorylating histone H2AX*. *Current Biology*, https://doi.org/10.1016/j.cub.2005.01.029.

Lu, H. and Davis, A.J., 2021. *Human RecQ Helicases in DNA Double-Strand Break Repair*. *Frontiers in Cell and Developmental Biology*, https://doi.org/10.3389/fcell.2021.640755.

Magni, M., Ruscica, V., Restelli, M., Fontanella, E., Buscemi, G. and Zannini, L., 2015. CCAR2/DBC1 is required for Chk2-dependent KAP1 phosphorylation and repair of DNA damage. *Oncotarget*, 6(19). https://doi.org/10.18632/oncotarget.4417.

Menolfi, D. and Zha, S., 2020. *ATM, ATR and DNA-PKcs kinases-the lessons from the mouse models: Inhibition = deletion*. *Cell and Bioscience*, https://doi.org/10.1186/s13578-020-0376-x.

Mirza-Aghazadeh-Attari, M., Mohammadzadeh, A., Yousefi, B., Mihanfar, A., Karimian, A. and Majidinia, M., 2019. *53BP1: A key player of DNA damage response with critical functions in cancer*. *DNA Repair*, https://doi.org/10.1016/j.dnarep.2018.11.008.

Murai, J., Huang, S.Y.N., Das, B.B., Renaud, A., Zhang, Y., Doroshow, J.H., Ji, J., Takeda, S. and Pommier, Y., 2012. Trapping of PARP1 and PARP2 by clinical PARP inhibitors. *Cancer Research*, 72(21). https://doi.org/10.1158/0008-5472.CAN-12-2753.

Nijman, S.M.B., 2011. *Synthetic lethality: General principles, utility and detection using genetic screens in human cells*. *FEBS Letters*, https://doi.org/10.1016/j.febslet.2010.11.024.

Nojadeh, J.N., Sharif, S.B. and Sakhinia, E., 2018. *Microsatellite instability in colorectal cancer*. *EXCLI Journal*, https://doi.org/10.17179/excli2017-948.

Noon, A.T., Shibata, A., Rief, N., Löbrich, M., Stewart, G.S., Jeggo, P.A. and Goodarzi, A.A., 2010. 53BP1-dependent robust localized KAP-1 phosphorylation is essential for

heterochromatic DNA double-strand break repair. *Nature Cell Biology*, 12(2). https://doi.org/10.1038/ncb2017.

Noordermeer, S.M., Adam, S., Setiaputra, D., Barazas, M., Pettitt, S.J., Ling, A.K., Olivieri, M., Álvarez-Quilón, A., Moatti, N., Zimmermann, M., Annunziato, S., Krastev, D.B., Song, F., Brandsma, I., Frankum, J., Brough, R., Sherker, A., Landry, S., Szilard, R.K., Munro, M.M., McEwan, A., de Rugy, T.G., Lin, Z.Y., Hart, T., Moffat, J., Gingras, A.C., Martin, A., van Attikum, H., Jonkers, J., Lord, C.J., Rottenberg, S. and Durocher, D., 2018. The shieldin complex mediates 53BP1-dependent DNA repair. *Nature*, 560(7716). https://doi.org/10.1038/s41586-018-0340-7.

O'Connor, M.J., 2015. *Targeting the DNA Damage Response in Cancer*. *Molecular Cell*, https://doi.org/10.1016/j.molcel.2015.10.040.

Panier, S. and Boulton, S.J., 2014. *Double-strand break repair: 53BP1 comes into focus*. *Nature Reviews Molecular Cell Biology*, https://doi.org/10.1038/nrm3719.

Patil, M., Pabla, N. and Dong, Z., 2013. *Checkpoint kinase 1 in DNA damage response and cell cycle regulation*. *Cellular and Molecular Life Sciences*, https://doi.org/10.1007/s00018-013-1307-3.

Peña-Diaz, J., Bregenhorn, S., Ghodgaonkar, M., Follonier, C., Artola-Borán, M., Castor, D., Lopes, M., Sartori, A.A. and Jiricny, J., 2012. Noncanonical Mismatch Repair as a Source of Genomic Instability in Human Cells. *Molecular Cell*, 47(5). https://doi.org/10.1016/j.molcel.2012.07.006.

Podhorecka, M., Skladanowski, A. and Bozko, P., 2010. *H2AX phosphorylation: Its role in DNA damage response and cancer therapy*. *Journal of Nucleic Acids*, https://doi.org/10.4061/2010/920161.

Pommier, Y., O'Connor, M.J. and de Bono, J., 2016. *Laying a trap to kill cancer cells: PARP inhibitors and their mechanisms of action*. *Science Translational Medicine*, https://doi.org/10.1126/scitranslmed.aaf9246.

Prakash, R., Zhang, Y., Feng, W. and Jasin, M., 2015. Homologous recombination and human health: The roles of BRCA1, BRCA2, and associated proteins. *Cold Spring Harbor Perspectives in Biology*, 7(4). https://doi.org/10.1101/cshperspect.a016600.

Qiu, Z., Oleinick, N.L. and Zhang, J., 2018. *ATR/CHK1 inhibitors and cancer therapy*. *Radiotherapy and Oncology*, https://doi.org/10.1016/j.radonc.2017.09.043.

Ranjha, L., Howard, S.M. and Cejka, P., 2018. *Main steps in DNA double-strand break repair: an introduction to homologous recombination and related processes*. *Chromosoma*, https://doi.org/10.1007/s00412-017-0658-1.

Redon, C.E., Nakamura, A.J., Zhang, Y.W., Ji, J., Bonner, W.M., Kinders, R.J., Parchment, R.E., Doroshow, J.H. and Pommier, Y., 2010. *Histone γH2AX and poly(ADP-ribose) as clinical pharmacodynamic biomarkers*. *Clinical Cancer Research*, https://doi.org/10.1158/1078-0432.CCR-10-0523.

Robertson, A.B., Klungland, A., Rognes, T. and Leiros, I., 2009. *Base excision repair: The long and short of it*. *Cellular and Molecular Life Sciences*, https://doi.org/10.1007/s00018-009-8736-z.

Roques, C., Coulombe, Y., Delannoy, M., Vignard, J., Grossi, S., Brodeur, I., Rodrigue, A., Gautier, J., Stasiak, A.Z., Stasiak, A., Constantinou, A. and Masson, J.Y., 2009. MRE11-RAD50-NBS1 is a critical regulator of FANCD2 stability and function during

DNA double-strand break repair. *EMBO Journal*, 28(16). https://doi.org/10.1038/emboj.2009.193.

Sancar, A., Lindsey-Boltz, L.A., Ünsal-Kaçmaz, K. and Linn, S., 2004. *Molecular mechanisms of mammalian DNA repair and the DNA damage checkpoints*. *Annual Review of Biochemistry*, https://doi.org/10.1146/annurev.biochem.73.011303.073723.

Sartori, A.A., Lukas, C., Coates, J., Mistrik, M., Fu, S., Bartek, J., Baer, R., Lukas, J. and Jackson, S.P., 2007. Human CtIP promotes DNA end resection. *Nature*, 450(7169). https://doi.org/10.1038/nature06337.

Scully, R., Panday, A., Elango, R. and Willis, N.A., 2019. *DNA double-strand break repair-pathway choice in somatic mammalian cells*. *Nature Reviews Molecular Cell Biology*, https://doi.org/10.1038/s41580-019-0152-0.

Seol, J.H., Shim, E.Y. and Lee, S.E., 2018. *Microhomology-mediated end joining: Good, bad and ugly*. *Mutation Research - Fundamental and Molecular Mechanisms of Mutagenesis*, https://doi.org/10.1016/j.mrfmmm.2017.07.002.

Shechter, D., Costanzo, V. and Gautier, J., 2004. *Regulation of DNA replication by ATR: Signaling in response to DNA intermediates*. *DNA Repair*, https://doi.org/10.1016/j.dnarep.2004.03.020.

Shi, W., Feng, Z., Zhang, J., Gonzalez-Suarez, I., Vanderwaal, R.P., Wu, X., Powell, S.N., Roti Roti, J.L., Gonzalo, S. and Zhang, J., 2010. The role of RPA2 phosphorylation in homologous recombination in response to replication arrest. *Carcinogenesis*, 31(6). https://doi.org/10.1093/carcin/bgq035.

Shiloh, Y., 2003. *ATM and related protein kinases: Safeguarding genome integrity*. *Nature Reviews Cancer*, https://doi.org/10.1038/nrc1011.

Shrivastav, M., de Haro, L.P. and Nickoloff, J.A., 2008. Regulation of DNA double-strand break repair pathway choice. *Cell Research*, 18(1). https://doi.org/10.1038/cr.2007.111.

Stark, J.M., Pierce, A.J., Oh, J., Pastink, A. and Jasin, M., 2004. Genetic Steps of Mammalian Homologous Repair with Distinct Mutagenic Consequences. *Molecular and Cellular Biology*, 24(21). https://doi.org/10.1128/mcb.24.21.9305-9316.2004.

Stiff, T., O'Driscoll, M., Rief, N., Iwabuchi, K., Löbrich, M. and Jeggo, P.A., 2004. ATM and DNA-PK Function Redundantly to Phosphorylate H2AX after Exposure to Ionizing Radiation. *Cancer Research*, 64(7). https://doi.org/10.1158/0008-5472.CAN-03-3207.

Vaksman, Z. and Garner, H.R., 2015. Somatic microsatellite variability as a predictive marker for colorectal cancer and liver cancer progression. *Oncotarget*, 6(8). https://doi.org/10.18632/oncotarget.3306.

Vassin, V.M., Wold, M.S. and Borowiec, J.A., 2004. Replication Protein A (RPA) Phosphorylation Prevents RPA Association with Replication Centers. *Molecular and Cellular Biology*, 24(5). https://doi.org/10.1128/mcb.24.5.1930-1943.2004.

Vítor, A.C., Huertas, P., Legube, G. and de Almeida, S.F., 2020. *Studying DNA Double-Strand Break Repair: An Ever-Growing Toolbox*. *Frontiers in Molecular Biosciences*, https://doi.org/10.3389/fmolb.2020.00024.

Wallace, S.S., 2014. Base excision repair: A critical player in many games. *DNA Repair*, 19. https://doi.org/10.1016/j.dnarep.2014.03.030.

Wang, H., Guan, J., Wang, H., Perrault, A.R., Wang, Y. and Iliakis, G., 2001. Replication protein A2 phosphorylation after DNA damage by the coordinated action of ataxia telangiectasia-mutated and DNA-dependent protein kinase. *Cancer Research*, 61(23).

Ward, I.M., Minn, K., van Deursen, J. and Chen, J., 2003. p53 Binding Protein 53BP1 Is Required for DNA Damage Responses and Tumor Suppression in Mice. *Molecular and Cellular Biology*, 23(7). https://doi.org/10.1128/mcb.23.7.2556-2563.2003.

Waskiewicz, E., Vasiliou, M., Corcoles-Saez, I. and Cha, R.S., 2021. Cancer genome datamining and functional genetic analysis implicate mechanisms of ATM/ATR dysfunction underpinning carcinogenesis. *Communications Biology*, 4(1). https://doi.org/10.1038/s42003-021-01884-x.

Weber, A.M. and Ryan, A.J., 2015. *ATM and ATR as therapeutic targets in cancer*. *Pharmacology and Therapeutics*, https://doi.org/10.1016/j.pharmthera.2014.12.001.

White, D., Rafalska-Metcalf, I.U., Ivanov, A. v., Corsinotti, A., Peng, H., Lee, S.C., Trono, D., Janicki, S.M. and Rauscher, F.J., 2012. The ATM substrate KAP1 controls DNA repair in heterochromatin: Regulation by HP1 proteins and serine 473/824 phosphorylation. *Molecular Cancer Research*, 10(3). https://doi.org/10.1158/1541-7786.MCR-11-0134.

Wilsker, D.F., Barrett, A.M., Dull, A.B., Lawrence, S.M., Hollingshead, M.G., Chen, A., Kummar, S., Parchment, R.E., Doroshow, J.H. and Kinders, R.J., 2019. Evaluation of pharmacodynamic responses to cancer therapeutic agents using DNA damage markers. *Clinical Cancer Research*, 25(10). https://doi.org/10.1158/1078-0432.CCR-18-2523.

Wright, W.D., Shah, S.S. and Heyer, W.D., 2018. *Homologous recombination and the repair of DNA double-strand breaks*. *Journal of Biological Chemistry*, https://doi.org/10.1074/jbc.TM118.000372.

Yang, G., Zheng, R. yi and Jin, Z. shun, 2019. *Correlations between microsatellite instability and the biological behaviour of tumours*. *Journal of Cancer Research and Clinical Oncology*, https://doi.org/10.1007/s00432-019-03053-4.

Zhao, W., Steinfeld, J.B., Liang, F., Chen, X., Maranon, D.G., Jian Ma, C., Kwon, Y., Rao, T., Wang, W., Sheng, C., Song, X., Deng, Y., Jimenez-Sainz, J., Lu, L., Jensen, R.B., Xiong, Y., Kupfer, G.M., Wiese, C., Greene, E.C. and Sung, P., 2017. BRCA1-BARD1 promotes RAD51-mediated homologous DNA pairing. *Nature*, 550(7676). https://doi.org/10.1038/nature24060.

Zhao, W., Vaithiyalingam, S., San Filippo, J., Maranon, D.G., Jimenez-Sainz, J., Fontenay, G. v., Kwon, Y., Leung, S.G., Lu, L., Jensen, R.B., Chazin, W.J., Wiese, C. and Sung, P., 2015. Promotion of BRCA2-Dependent Homologous Recombination by DSS1 via RPA Targeting and DNA Mimicry. *Molecular Cell*, 59(2). https://doi.org/10.1016/j.molcel.2015.05.032.

Zheng, F., Zhang, Y., Chen, S., Weng, X., Rao, Y. and Fang, H., 2020. *Mechanism and current progress of Poly ADP-ribose polymerase (PARP) inhibitors in the treatment of ovarian cancer*. *Biomedicine and Pharmacotherapy*, https://doi.org/10.1016/j.biopha.2019.109661.

Ziv, Y., Bielopolski, D., Galanty, Y., Lukas, C., Taya, Y., Schultz, D.C., Lukas, J., Bekker-Jensen, S., Bartek, J. and Shiloh, Y., 2006. Chromatin relaxation in response to DNA

double-strand breaks is modulated by a novel ATM-and KAP-1 dependent pathway. *Nature Cell Biology*, 8(8). https://doi.org/10.1038/ncb1446.

Appendices

Appendix 1. Nuclei count and size after MMC treatment

Cell proliferation was monitored during these experiments (Figure 22A). With both cell lines 1000 nM MMC inhibited the proliferation. After MMC treatment with the 1000 nM concentration at 24 h timepoint an increase in nuclei size was observed as well (Figure 22B). This increase was significant in parental cells where the increase was almost fourfold at 72 h timepoint.

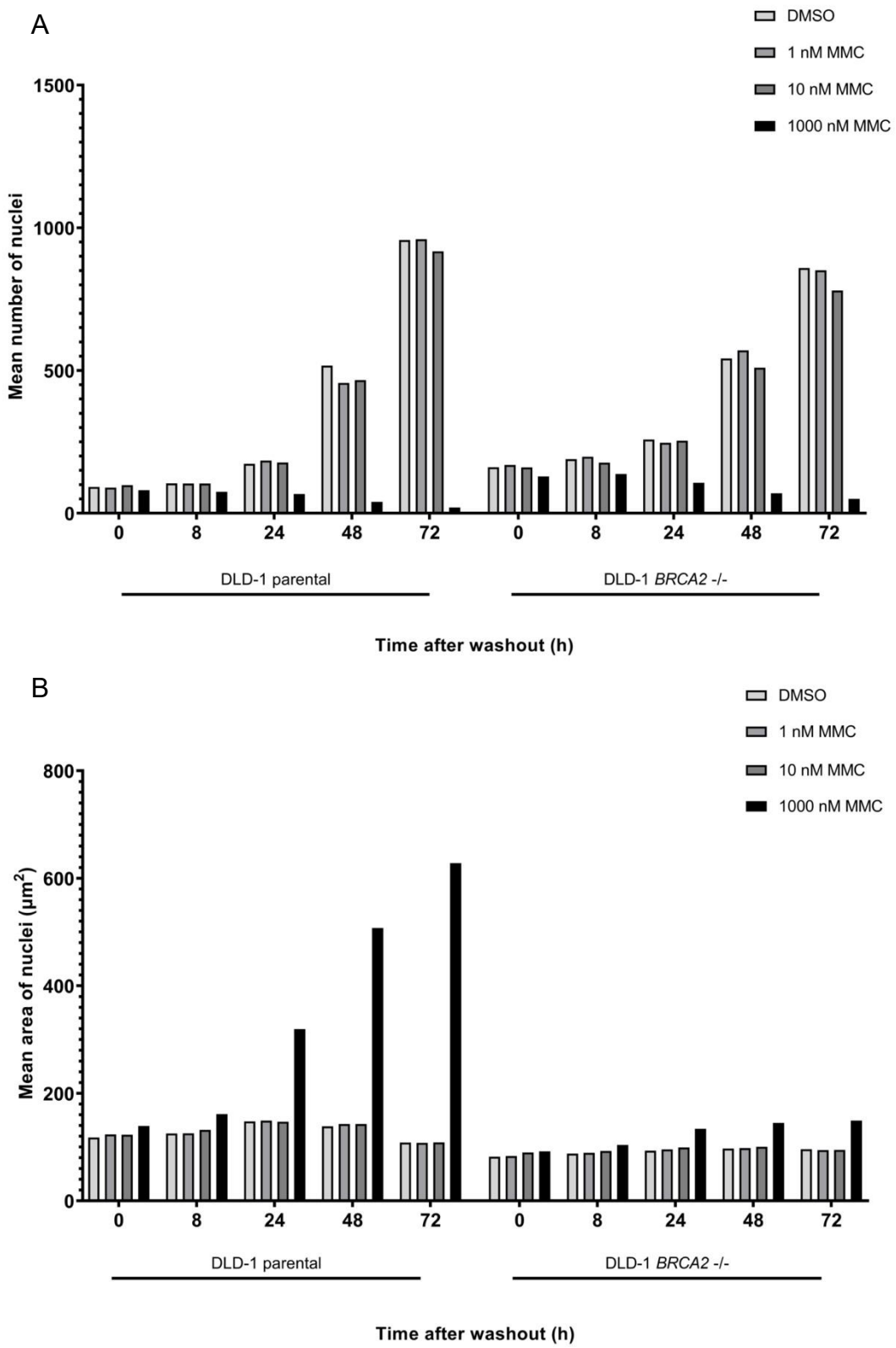

Figure 22. (A) Mean number and (B) mean area of nuclei in parental and KO cells after treatment with MMC. Results represent the mean of individual representative experiment.

Appendix 2. Nuclei count and size after ATRi and PARPi treatment

After ATRi and PARPi treatment differences in nuclei count was observed only with treatment with 1000 nM elimusertib. With all the other compounds and concentration cells were able to proliferate throughout the study (Figure 23A). Similar increase in nuclei size as was noted in MMC experiments was not observed in these experiments (Figure 23B).

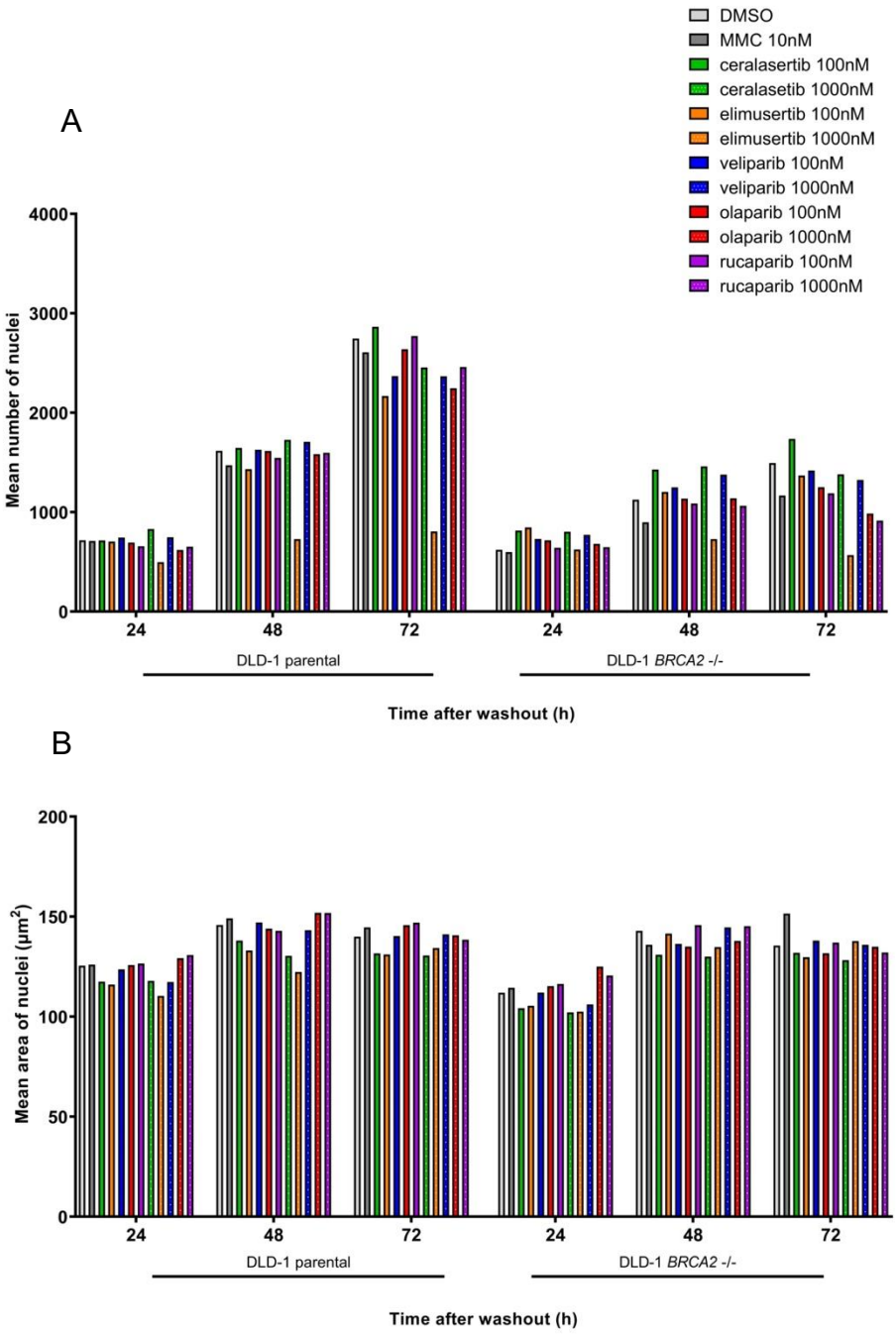

Figure 23. (A) Mean number and (B) mean area of nuclei in parental and KO cells after treatment with PARP and ATR inhibitors. Results represent the mean of individual representative experiment.